



ALMA MATER STUDIORUM
UNIVERSITÀ DI BOLOGNA

ARCHIVIO ISTITUZIONALE
DELLA RICERCA

Alma Mater Studiorum Università di Bologna Archivio istituzionale della ricerca

Lignin-derived bimetallic platinum group metal-free oxygen reduction reaction electrocatalysts for acid and alkaline fuel cells

This is the final peer-reviewed author's accepted manuscript (postprint) of the following publication:

Published Version:

Muhyuddin, M., Friedman, A., Poli, F., Petri, E., Honig, H., Basile, F., et al. (2023). Lignin-derived bimetallic platinum group metal-free oxygen reduction reaction electrocatalysts for acid and alkaline fuel cells. *JOURNAL OF POWER SOURCES*, 556, 1-12 [10.1016/j.jpowsour.2022.232416].

Availability:

This version is available at: <https://hdl.handle.net/11585/915070> since: 2024-09-11

Published:

DOI: <http://doi.org/10.1016/j.jpowsour.2022.232416>

Terms of use:

Some rights reserved. The terms and conditions for the reuse of this version of the manuscript are specified in the publishing policy. For all terms of use and more information see the publisher's website.

This item was downloaded from IRIS Università di Bologna (<https://cris.unibo.it/>).
When citing, please refer to the published version.

(Article begins on next page)

17
18 10 **Lignin-derived bimetallic platinum group metal-free oxygen reduction reaction**
19 11 **electrocatalysts for acid and alkaline fuel cells**
20 12

21 13 Mohsin Muhyuddin¹, Ariel Friedman², Federico Poli³, Elisabetta Petri³, Hilah Honig², Francesco
22 14 Basile⁴, Andrea Fasolini⁴, Roberto Lorenzi¹, Enrico Berretti⁵, Marco Bellini⁵, Alessandro
23 15 Lavacchi⁵, Lior Elbaz², *Carlo Santoro¹, **Francesca Soavi³
24 16

25 17
26 18 ¹Department of Materials Science, University of Milano-Bicocca, Via Cozzi 55, Building U5,
27 19 20126 Milan, Italy

28 20 ² Department of Chemistry and the Institute of Nanotechnology and Advanced Materials, Bar-Ilan
29 21 University, Ramat-Gan 5290002, Israel

30 22 ³Department of Chemistry “Giacomo Ciamician”, Alma Mater Studiorum – Università di
31 23 Bologna, Italy

32 24 ⁴ Department of Industrial Chemistry “Toso Montanari”, Alma Mater Studiorum – Università di
33 25 Bologna, Italy

34 26 ⁵ Istituto di Chimica Dei Composti OrganoMetallici (ICCOM), Consiglio Nazionale Delle
35 27 Ricerche (CNR), Via Madonna Del Piano 10, 50019 Sesto Fiorentino, Firenze, Italy

36 28 * Carlo Santoro: carlo.santoro@unimib.it

37 29 ** Francesca Soavi: francesca.soavi@unibo.it

38 30 **Abstract**

39 31 Metal-nitrogen-carbons (M-N-Cs) as a reliable substitution for platinum-group-metals (PGMs) for
40 32 oxygen reduction reaction (ORR) are emerging candidates to rationalize the technology of fuel
41 33 cells. The development of M-N-Cs can further be economized by consuming waste biomass as an
42 34 inexpensive carbon source for the electrocatalyst support. Herein, we report the simple fabrication
43 35 and in-depth characterization of electrocatalysts using lignin-derived activated char. The activated
44 36 char (LAC) was functionalized with phthalocyanine (FePc and MnPc) via atmosphere-controlled
45 37 pyrolysis to produce monometallic M-N-Cs (L_Mn and L_Fe) and bimetallic M1-M2-N-Cs
46 38 (L_FeMn) electrocatalysts. Raman spectroscopy and transmission electron microscopy (TEM)
47 39 revealed a defect-rich architecture. XPS confirmed the coexistence of various nitrogen-containing
48 40 active moieties. L_Fe and L_FeMn demonstrated appreciable ORR in both acidic and alkaline
49 41 conditions whereas L_FeMn helped in restricting the peroxide yield, particularly in alkaline media.
50 42 L_Fe and L_FeMn demonstrated remarkable onset potential (E_{onset}) of ~0.942V (vs RHE) with an
51 43 $E_{1/2}$ of 0.874V (vs RHE) in 0.1M KOH. In acid, L_FeMn had an E_{onset} of 0.817V (vs RHE) and an

1
2
3
4 1 $E_{1/2}$ of $\sim 0.76\text{V}$ (vs RHE). Finally, the L_FeMn cathode electrocatalyst was integrated and tested in
5
6 2 PEMFC and AEMFC. AEMFC demonstrated optimistic performance with a peak power density
7
8 3 of 261 mW cm^{-2} at the current density of $\sim 577\text{ mA cm}^{-2}$.
9

10 4
11 5 **Keywords:** lignin-derived char, oxygen reduction reaction, platinum group metal-free, proton
12 6 exchange membrane fuel cell, anion exchange membrane fuel cell
13
14
15 7

16 8 **1. Introduction**

19 9 Low-temperature fuel cells (FCs) being capable of converting chemical energy into electrical
20
21 10 energy without contributing to planetary carbon footprints are one of the most paramount
22
23 11 candidates to sustainably address the global energy crises. Within the paradigm of advanced FCs,
24
25 12 analogous technologies of proton exchange membrane FCs (PEMFCs) and anion-exchange-
26
27 13 membrane FCs (AEMFCs) are capturing scientific attention owing to their unique merits. Both
28
29 14 technologies with different pH of electrolytic media realize the incessant translation of energy
30
31 15 through hydrogen oxidation reaction (HOR) at the anode and the oxygen reduction reaction (ORR)
32
33 16 at the cathode, leaving water as a green byproduct. However, even though FCs are having
34
35 17 considerable commercial success, the complex and lethargic ORR constitutes the key hindrance in
36
37 18 their practical deployment on a large scale since it is several orders of magnitude slower than the
38
39 19 HOR [1–3]. Reduction of oxygen follows multielectron transfer routes with sluggish kinetics,
40
41 20 imposing much higher overpotential and thus restricting the overall device efficiency. It is known
42
43 21 in the scientific community that ORR usually proceeds either in a bi-electronic or tetra-electronic
44
45 22 fashion producing peroxide or water, respectively [4–8]. From the perspective of FCs, the tetra-
46
47 23 electronic pathway is essentially important whereas the production of highly reactive peroxide
48
49 24 during bi-electronic ORR not only makes the system less energy efficient but also severely affects
50
51 25 the integrity of membrane electrode assembly (MEA) and stack architecture. To deal with the
52
53 26 aforementioned challenges, platinum group metals (PGMs) are typically employed which
54
55 27 eventually make the application of FCs economically impracticable. The use of scarce and
56
57 28 expensive Pt in the fabrication of ORR electrocatalysts accounts for more than 55% of the total
58
59 29 cost of an FC stack [9,10]. Moreover, state-of-the-art Pt-based electrocatalysts are also notorious
60
61 30 for their undesired dissolution, nanoparticle coalescence and poisoning with common
62
63 31 contaminants which in turn gravely diminish the electrocatalytic efficiency [10,11]. Therefore, it
64
65

1 is an urgent need of the hour to cope with such complications either by reducing the Pt content or
2 by substituting with PGM-free electrocatalysts. In the pursuit of PGM-free electrocatalysis, metal-
3 nitrogen-carbons (M-N-Cs, M=Mn, Fe, Co, Ni etc.) are emerging as a reliable competitor in which
4 earth-abundant transition metals (TM) having coordination with different nitrogen species (MN_x)
5 make active moieties for ORR within the porous carbonaceous framework [6,12–17].

6 In the search for an efficacious M-N-C electrocatalyst, various designing parameters must
7 be considered. First comes the porous nature of carbonaceous architecture. Carbon provides a
8 conducive platform for the whole electrochemical activity whereas a high surface area and
9 mesoporous environment boost the mass transport of gaseous reagents to the active sites[18].
10 Where the intrinsic defects, ruptured facets and structural discontinuities in carbon facilitate the
11 binding of oxygen [19], the dangling bonds present in the unsaturated vacancies also contribute to
12 the doping of secondary elements i.e. nitrogen to generate the active moieties [20]. Furthermore,
13 nitrogen doping breaks the electro-neutrality of the carbon triggering the chemisorption of O_2 [21]
14 and due to enhanced Lewis basicity, pyridinic-nitrogen effectively participates in ORR by
15 subsequently reducing the peroxide intermediate into water [22,23]. Over and above that, the
16 selection of the transition metal is a strategic task in electrocatalyst development as the electrons
17 transfer from metal to oxygen is primarily dictated by the redox potential of the central metal
18 [16,24–26] and hence the plurality of redox sites is one of the foremost prerequisites for O_2
19 activation and the subsequent reduction [16]. MN_x ($x=2,3,4$) is undoubtedly the most
20 electrocatalytically active site in which a central TM atom has coordination with pyridinic nitrogen
21 ligands on the distorted carbon surface and aptly bio-mimic the natural enzyme to reduce oxygen
22 [27–30]. In addition to the conventional exploitation of metal salts and organic precursors of
23 nitrogen and carbon for the fabrication of M-N-Cs, the use of metal macrocyclic compounds i.e.
24 metal phthalocyanine (MPc) and porphyrins have the preferred MN_4 sites. However, a
25 thermomechanical treatment known as pyrolysis becomes inevitably imperative to achieve the
26 mandatory durability and robustness. This occurs by integrating the MN_4 active site onto the
27 carbon backbone, favored by the high-temperature treatment. Although such active sites can be
28 generated using MPc of different first-row TM, Fe- N_4 finds its place at the apex of the volcano
29 curve due to its moderate adsorption portfolio [13,16,24,25,31]. It is noteworthy that FePc and
30 MnPc promote the tetra-electronic ORR by rupturing the O-O bond due to the preferable ‘*d*

1
2
3
4 1 *character*'. On the other hand, it was shown that CoPc, NiPc and CuPc tend to catalyze the ORR
5
6 2 in a bi-electronic manner, underlined by the high intermediate production measured [16,24,31,32].
7

8 3 Notwithstanding the fact that Fe-N-Cs are glossing in the arena of PGM-free
9
10 4 electrocatalysis, their performance is still inferior compared to PGM-based electrocatalysts,
11 5 spurring extensive global ventures to understand and improve the activity of Fe-N-Cs [33–39]. To
12 6 mitigate the efficiency pitfalls, the introduction of a second TM could be useful [40]. Serov et al.
13 7 analyzed the influence of Fe interaction with a second TM by developing a series of
14 8 electrocatalysts using a sacrificial support method (SSM) and observed a substantial upturn in
15 9 ORR activity after the addition of a second TM [41]. At the present, some acknowledgeable efforts
16 10 have been made to co-doped Fe and Co [42–46]. However, again the usage of Co challenges the
17 11 economic rationalization of FCs since it is listed among critical raw materials[47,48] and also Co
18 12 holds the tendency of producing higher peroxide [17,49]. Moreover, as compared to Co, the
19 13 supplementation of Mn into Fe-carrying M-N-Cs clearly improves the electrocatalytic activity by
20 14 keeping the peroxide generation relatively lower which ultimately hastens up the cathodic
21 15 performance [50–52].
22
23
24
25
26
27
28
29
30
31

32 16 In parallel, a growing scientific interest has recently been witnessed in the development of
33 17 ORR electrocatalysts using waste biomasses [53–59] and plastics [60–64] as a cheaper and readily
34 18 available source of carbon and such initiatives could circularly ensure ecological safety. Global
35 19 agricultural waste generation is gigantically increasing on annual basis [65] and hence, its
36 20 transformation into innovative materials is rationally justified considering the environmental gains
37 21 of waste reduction [53]. As already mentioned, porosity and high surface area are primarily
38 22 required for providing accessibility to the active sites, biomasses owing to trimodal structures
39 23 efficiently fulfill this prerequisite and act as a tailorable pattern for novel materials
40 24 fabrication[55,66]. Among these biomass wastes, lignin derived from waste biomass is one of the
41 25 most produced agricultural wastes. According to an estimation, annual global harvesting of
42 26 biomass accounts for more than 170 billion metric tons [67] out of which lignin is present up to
43 27 25% [68] whereas the pulp and paper industry generates up to 50-70 million tons per year [69,70]
44 28 which is expected to surpass the figure of 225 million tons annually by the year 2030 [70,71].
45
46
47
48
49
50
51
52
53
54
55

56 29 Herein, within the core of the circular economy, we valorize real waste lignin and transform
57 30 it through pyrolysis and activation processes into high surface area char that is then functionalized
58 31 with mono- and bi-metallic phthalocyanine and tested as PGM-free electrocatalyst for oxygen
59
60
61
62
63
64
65

1
2
3
4 1 reduction reaction in acid and alkaline media. After a complete physio-chemical and
5
6 2 electrochemical characterization, the lignin-derived PGM-free electrocatalysts are integrated into
7
8 3 cathode electrodes and tested in PEMFC and AEMFC.
9

10 4 11 5 **2. Materials and Methods**

12 13 6 **2.1. Lignin Derived Activated Char (LAC)**

14
15 7 Lignin-derived Activated Char (LAC) was produced by adapting the process reported in ref [59].
16
17 8 The raw lignin, a real solid waste of an anaerobic biodigester plant located in Bologna (Biotec Sys
18
19 9 srl), was washed with a water/ethanol mixture and then dispersed in an aqueous solution with a
20
21 10 mild activating agent, KHCO_3 for 24 h (1:2 of Lignin: KHCO_3 in ratio). The dried mold was kept
22
23 11 in two identical grids, placed in a Tubular Oven (ELITE TSH16/50/610-2216E) and pyrolyzed
24
25 12 under N_2 flux by heating from room temperature to 850°C and held for 1 h while keeping the
26
27 13 heating and then left to cool down. The biochar resulting from the two grids was mixed and sieved
28
29 14 before proceeding with a deashing with 3 M HCl for 8 h and washing with deionized water under
30
31 15 a vacuum. In the end, soxhlet extraction with water was performed. The activated char (LAC)
32
33 16 produced featured a specific surface area of $1367 \text{ m}^2 \text{ g}^{-1}$.

34 35 18 **2.2. Electrocatalyst Synthesis**

36
37 19 The synthesis of electrocatalysts was carried out by functionalizing the (LAC) with the metal(s)-
38
39 20 phthalocyanine (MPc) of interest. To begin with, 80 wt.% of LAC was thoroughly mixed with 20
40
41 21 wt.% MPc. **Table 1** demonstrates the weight proportions of LAC and MPc set to fabricate
42
43 22 monometallic and bimetallic samples. The homogenized mixture obtained in the first step was then
44
45 23 transferred into a clean ceramic boat and subjected to a controlled atmosphere tube furnace
46
47 24 (Carbolite) for high-temperature pyrolysis. During the pyrolysis, the material was taken from room
48
49 25 temperature to 600°C and held there for 1 h while keeping the heating and cooling ramp rates at
50
51 26 5°C min^{-1} . Whereas the whole process was performed in 5 wt.% H_2 balanced with N_2 at 100 cm^3
52
53 27 min^{-1} . Afterward, the obtained electrocatalyst was rigorously homogenized by giving a round of
54
55 28 ball milling (E_{MAX} , Retsch GmbH, Germany) at 400 rpm for 40 min using zirconia balls of 3 mm
56
57 29 diameter.
58
59 30
60
61
62
63
64
65

1
2
3
4 1 **Table 1.** Description of the samples studied.
5

Sample Names	LAC (Wt. %)	FePc (Wt. %)	MnPc (Wt. %)
LAC	100	--	--
L_Fe	80	20	--
L_Mn	80	--	20
L_FeMn	80	10	10

17 2
18
19 3 **2.3. Structural and Morphological Characterization**
20

21 4 The textural properties of the LAC were evaluated by nitrogen adsorption porosimetry
22 5 measurements that were carried out at 77 K with an ASAP 2020 system (Micromeritics) after a
23 6 drying step for 24 h at 413 K. The Brunauer-Emmett-Teller (BET) and density functional (DFT)
24 7 theories were used to analyze N₂ adsorption isotherm, in order to obtain specific surface area (S_{BET})
25 8 and pores size distribution (PSD), respectively.
26 9

30 9 Thermogravimetry analysis (TGA) was conducted using TA Instrument TGA Q50
31 10 analyzer in the oxygen atmosphere, in order to evaluate the ash content of the LAC produced. The
32 11 analysis was performed by applying a temperature ramp of 10°C/min from RT to 850°C.
33 12

34 12 Energy-dispersive X-ray fluorescence (XRF) having an X-ray tube with a molybdenum anode
35 13 (Bruker Artax 200 spectrometer) was utilized to perform qualitative elemental analysis. For the
36 14 crystal structure evaluation, X-ray diffraction (XRD, Rigaku Miniflex 600) with a copper source
37 15 was employed in the 2θ range of 10-90°. To investigate the carbonaceous structure of as-developed
38 16 electrocatalysts, Raman spectroscopy (LabRam, Jobin Yvon, France) was utilized where helium-
39 17 neon laser (λ=632.8 nm) as an excitation source was focused on the sample with the help of BX40
40 18 microscope (Olympus, Japan) while a silicon-based CCD system (Sincerity, Jobin Yvon, France)
41 19 was used to collect the signals.
42 20

43 20 X-ray photoelectron spectroscopy (XPS) was carried out using a Nexsa spectrometer
44 21 (England) equipped with a monochromatic, micro-focused, lower Al Ka X-ray (photon energy
45 22 1486.6 eV). Survey and high-resolution spectra were acquired at pass energy of 200 eV and 50
46 23 eV, respectively. The source power was normally 72W. All elements' binding energies were
47 24 recalibrated by setting the CC/CH component of the adventitious carbon 1st peak at 285 eV. The
48 25 measurements were carried out under UHV conditions, at a base pressure of 5x10⁻¹⁰ torr (and no
49 50
51
52
53
54
55
56
57
58
59
60
61
62
63
64
65

1 higher than 3×10^{-9} torr). Data analysis was performed using AVANTAGE software. Linear
2 background subtraction was used for all spectra. High-Resolution Transmission electron
3 microscopy (HRTEM) measurements were done using, JEOL JEM 2100, LaB6 filament, 200 kV.

4 5 **2.4. Electrochemical Analysis**

6 The kinetic parameters of the developed electrocatalysts were investigated through the rotating
7 ring disk electrode (RRDE) methodology (Pine WaveVortex RDE connected with a Pine
8 bipotentiostat). For the preparation of inks, 5 mg of the synthesized electrocatalyst was suspended
9 in a solution containing 985 μL of isopropanol (Alfa Aesar) and 15 μL of 5 wt.% Nafion[®] D-520
10 (Alfa Aesar). The inks were homogenized by probe sonication for 10 mins followed by ultrasonic
11 bath sonication for the next 30 mins at ambient temperature. E6R2 series RRDE electrode was
12 used to fabricate the working electrode with 0.2 mg cm^{-2} and 0.6 mg cm^{-2} loadings of each
13 electrocatalyst. In-house prepared 0.5 M H_2SO_4 and 0.1 M KOH solutions were used as the
14 electrolytic media in O_2 -saturated circumstances to simulate ORR activity in acidic and alkaline
15 conditions, respectively. The experiments were run in a three-electrode configuration
16 encompassing a Pt-based counter electrode, saturated calomel electrode (SCE) as a reference and
17 RRDE working electrode while 85% IR compensations were made using SP-100 Biologic[®]
18 potentiostat. In this study, all the potentials are presented with respect to reversible hydrogen
19 potential (RHE) after adding a factor of $0.241 + \text{pH} \times 0.0591$ into the measured potentials which
20 were originally referenced to SCE. Linear sweep voltammetry (LSV) was executed to acquire
21 polarization curves at 5 mV s^{-1} between 1200 and 0 mV vs RHE while maintaining the ring
22 potential $\sim 1200 \text{ mV vs RHE}$. ORR measurements were performed by rotating the RRDE at 1600
23 rpm. Before getting the actual LSV curves, the electrocatalyst was conditioned with multiple cyclic
24 voltammograms until a stable current was achieved. The peroxide yield and number of electron
25 transfers (n) during ORR were estimated by monitoring the disk current (I_{disk}) and ring current
26 (I_{ring}) using the following equations:

$$27 \text{ Peroxide (\%)} = \frac{200 \times \frac{I_{\text{ring}}}{N}}{I_{\text{disk}} + \frac{I_{\text{ring}}}{N}} \quad (\text{eq.1})$$

$$28 n = \frac{4 I_{\text{disk}}}{I_{\text{disk}} + \frac{I_{\text{ring}}}{N}} \quad (\text{eq.2})$$

1
2
3
4 1 The electrochemical stability was analyzed by applying 5000 cycles in the potential range between
5
6 2 1100 and 300 mV vs RHE at 50 mV s^{-1} in the O_2 -saturated electrolytes by rotating the RRDE (with
7
8 3 0.6 mg cm^{-2} electrocatalyst loading) at 1600 rpm. For making a comparison, ORR polarization
9
10 4 curves were obtained again at 5 mV s^{-1} .
11
12 5

13 6 **2.5. Fuel Cell Fabrication and Testing**

14 15 16 7 **2.5.1 AEMFC**

17
18 8 All AEMFC electrodes used in this work were prepared as described in detail in our previous
19
20 9 publications [72,73]. In brief, the electrocatalyst powder (80% wt.) was mixed with the ETFE-
21
22 10 based anion exchange ionomer powder (20% wt.) containing benzyl trimethylammonium (BTMA)
23
24 11 functional groups in 10 ml of distilled water and 2 propyl alcohol (1:1) solution. The resulting ink
25
26 12 was homogenized by 30 mins of ultrasound treatment (45 kHz, 100 W) and then sprayed using an
27
28 13 Iwata[®] spray gun onto the gas diffusion layer TGP-H-60 carbon paper 10% PTFE purchased by
29
30 14 Alfa Aesar. The catalyst spray was suspended every once in a while to dry the electrode for 10 sec
31
32 15 on an $80 \text{ }^\circ\text{C}$ hot plate and subsequently weighed to control the electrocatalyst correct loading. The
33
34 16 anode loading was ca. $0.4 \text{ mg}_{\text{PtRu}} \text{ cm}^{-2}$, the cathode coating was $0.8 \text{ mg}_{\text{electrocatalyst}} \text{ cm}^{-2}$.

35
36 17 The anion exchange membrane (AEM) preparation procedure has previously been
37
38 18 described in ref. [74] and consists of a $10 \text{ }\mu\text{M}$ HDPE sheet functionalized with vinylbenzyl chloride
39
40 19 monomer by electron-beam radiation grafting (100 kGy absorbed dose). The membrane was
41
42 20 subjected to amination treatment with aqueous TMA (45 wt %). The AEM and the electrodes were
43
44 21 immersed in 1 M KOH aqueous solution for 1 h before assembly into a 5 cm^2 fuel cell fixture
45
46 22 (Scribner Associates) using a 5 N m torque. The AEMFC was tested with a Scribner Associates
47
48 23 850e fuel cell test station setting the cell temperature at $60 \text{ }^\circ\text{C}$. The anode was fed with pure
49
50 24 hydrogen at $54 \text{ }^\circ\text{C}$ (75% relative humidity) at 0.3 L min^{-1} flow rate and the cathode was fed with
51
52 25 pure oxygen at $60 \text{ }^\circ\text{C}$ (100% relative humidity) at 0.6 L min^{-1} . The cell was characterized by
53
54 26 consecutive 20 scan voltage experiments from OCV to 0.3 V applying a 10 mV s^{-1} linear sweep.
55
56 27

57 58 59 60 28 **2.5.2 PEMFC**

61
62
63
64
65 29 The electrocatalyst (L_FeMn) was also tested in a PEM-FC. 152 mg of Nafion solution (D1021),
66
67 30 0.566 mL of isopropanol and 0.477 mL of water were added to 26 mg of the electrocatalyst. The
68
69 31 ink was sonicated for 1.5 h in ice. The electrocatalyst was sprayed on the 29BC gas diffusion layer

(GDL) using the airbrush. The final loading was $\sim 4.4 \text{ mg cm}^{-2}$. A commercial gas diffusion electrode (GDE) (Fuel Cells Etc., CST-GDE-01) of 0.2 mg cm^{-2} of Pt/C was used at the anode side. The anode GDE was hot pressed with NR-211 Nafion membrane ($130 \text{ }^\circ\text{C}$) for 5 min. Then, the cathode GDE was assembled without hot pressing the MEA. The cell was tightened up to 10 Nm.

The cell was operated at $80 \text{ }^\circ\text{C}$. For testing the MEA, hydrogen (0.5 L min^{-1}) and air (0.7 L min^{-1}) were used at the anode and cathode sides, respectively (both at $80 \text{ }^\circ\text{C}$). Break-in was performed by holding the cell at 0.15 mA cm^{-2} until the cell voltage was stabilized ($\sim 5 \text{ min}$). Then, the voltage was scanned between 0.0 to 0.7 V (0.025 A/point , 30 sec) and from 0.7 V to 0.2 V (0.05 A/point , 30 sec).

3. Results and Discussion

3.1. Initial Characterization of lignin Derived Activated Char

Black char was formed after the pyrolysis of the waste lignin. Importantly, initial screening evaluating the BET surface area (S_{BET}) and the ash content was conducted.

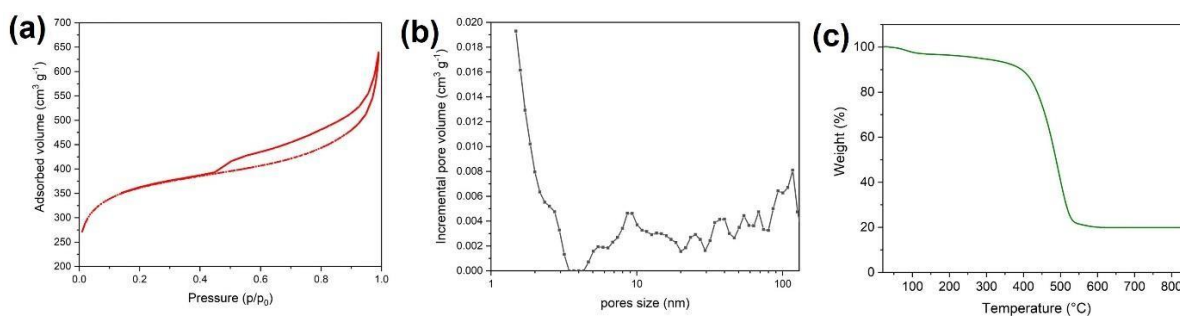


Figure 1. N_2 adsorption-desorption isotherms (a), pore size distribution (b) and thermogravimetric analysis (c) of LAC.

The evaluation of the surface area and pore size distribution was carried out by analyzing the N_2 adsorption/desorption isotherms at 77 K which is reported in [Figure 1a](#). At low pressures, the isotherm branch of the LAC sample illustrated sharp adsorption inflection which is indicative of type I and materials containing micropores. However, at higher relative pressures of $0.45 < P/P_0 < 1.0$, the presence of an H4 hysteresis loop indicates that LAC is a complex material containing interconnected micropores and mesopores (type IV).

1 These observations are confirmed by the DFT pore size distribution that is reported in terms of
 2 incremental pore volume in Figure 1b. The micropore volume (V_{micro}), mesopore volume (V_{meso})
 3 and total pore volume (V_{total}) of the sample is charted in Table 2 along with the BET surface area
 4 (S_{BET}). The S_{BET} is $1367 \pm 1 \text{ m}^2 \text{ g}^{-1}$. Such high value is mainly related to micropores and small
 5 mesopores ($< 3\text{nm}$). Indeed, V_{micro} ($0.40 \text{ cm}^3 \text{ g}^{-1}$) accounts for the 70% V_{total} ($0.57 \text{ cm}^3 \text{ g}^{-1}$). Larger
 6 pores are almost equally distributed from 3 nm up to more than 100 nm, and contribute with only
 7 the 20% to V_{total} ($V_{\text{meso}} = 0.12 \text{ cm}^3 \text{ g}^{-1}$).

8
 9 **Table 2.** DFT micropore volume (V_{micro}), mesopore volume (V_{meso}) and total pore volume (V_{total}),
 10 BET-specific surface area (S_{BET}) and ash content of LAC.

Sample	$V_{\text{micro}} (<2\text{nm})$ $\text{cm}^3 \text{ g}^{-1}$	$V_{\text{meso}} (2 -50 \text{ nm})$ $\text{cm}^3 \text{ g}^{-1}$	$V_{\text{total}} \text{ cm}^3 \text{ g}^{-1}$	S_{BET} $\text{m}^2 \text{ g}^{-1}$	Ash content (%)
LAC	0.40	0.12	0.57 ($< 137 \text{ nm}$)	1367 ± 1	19

11
 12
 13 Finally, Figure 1c reported the thermogravimetric analysis of the LAC produced. The ash content
 14 evaluated is reported in Table 2 and is about 19 %. This result may depend on the natural origin
 15 of the raw material.

16
 17 **3.2. Structural and Morphological Investigations**

1
2
3
4
5
6
7
8
9
10
11
12
13
14
15
16
17
18
19
20
21
22
23
24
25
26
27
28
29
30
31
32
33
34
35
36
37
38
39
40
41
42
43
44
45
46
47
48
49
50
51
52
53
54
55
56
57
58
59
60
61
62
63
64
65

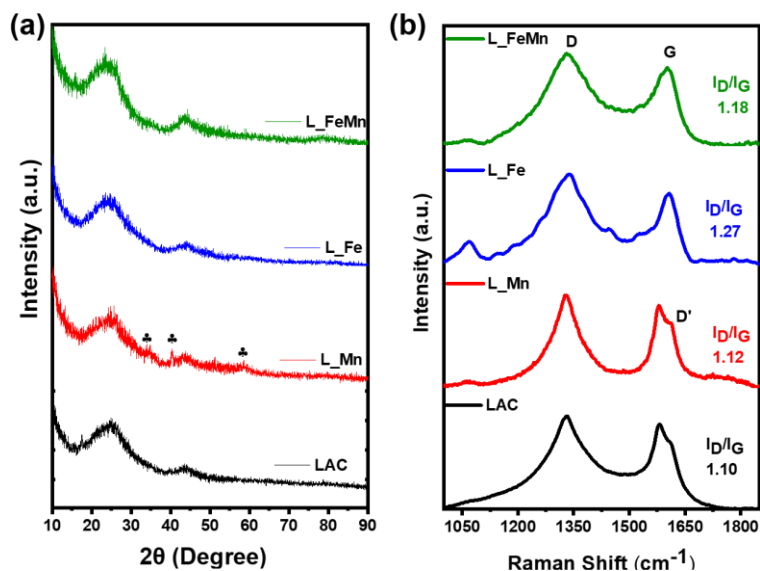


Figure 2. XRD patterns (a) and Raman spectra (b) of the as-developed samples.

Soon after the functionalization of the LAC with the MPC of interest, qualitative elemental analysis was carried out using XRF (Figure S1). Each sample showed clear peaks of the metal of interest i.e. Fe and/or Mn, justifying the effectiveness of the synthesis process. However, pristine LAC (Figure S1a) contained a few traces of Fe, Cu and Ni, which probably were present in the raw material or got introduced as contamination during the processing and therefore were minutely present in every sample. Since the relative presence of impurities was too low they were not considered contributors to ORR and were unheeded. Moreover, XRD was employed with the aim of phase identification and two broader peaks that emerged nearly at 25° and 43.5° were indexed to (002) and (101) planes of carbon, respectively, portending the distorted nature of the graphitic matrix [75,76] (Figure 2a). Only, sample L_Mn demonstrated very tiny peaks of MnO at ~34.9°, ~40.5° and ~58°, consistent with JPDs# 01-089-4835. Kumar et al. also experienced such tiny MnO peaks in the XRD pattern of bimetallic ORR electrocatalysts fabricated by dual functionalization of carbon nanotubes with FePc and MnPc [40]. However, quite interestingly, L_Fe and L_FeMn demonstrated only the diffraction peaks of carbon, giving an impression of the homogenized distribution of Fe and Mn-based species in the carbon matrix without forming coarser crystalline nanoparticles [76–79]. In our case, the usage of MPC in a relatively smaller proportion might have restricted the excessive coalescence of metallic species into coarser nanoparticles. Moreover, appreciable prevention of metal nanoclustering up to a pyrolysis

1 temperature of 600 °C has already been witnessed [80]. The carbonaceous structure of the resultant
2 electrocatalysts was further examined by the way of Raman spectroscopy as demonstrated in
3 [Figure 2b](#). All the samples revealed typical G (nearly at 1590 cm⁻¹) and D (nearly at 1330 cm⁻¹)
4 bands, due to in-plane stretching of the sp² carbon atom with E_{2g} symmetry and breathing mode of
5 A_{1g} symmetry, respectively [81,82]. LAC and L_Mn also exhibited a D' band in the vicinity of
6 1613 cm⁻¹. The G band is conventionally ascribed to graphitization content while the D and D'
7 band emerges because of the structural disruption and induced defects in the original lattice [81–
8 85]. It is worth mentioning that every sample had a higher D peak indicating a greater extent of
9 disorders and defects in the carbon architecture, which could substantially participate in enhancing
10 the ORR activity due to modified electronic and chemical characteristics of the disrupted carbons
11 [76,86,87]. As it is well known, the ratio of D to G band intensity (I_D/I_G) manifests the degree of
12 disorder in carbon-based materials. I_D/I_G remained always higher than unity where this intensity
13 ratio reached the maximum value of 1.27 for L_Fe followed by 1.18 for L_FeMn which indicates
14 the occurrence of a very high defect density.

3.3. Surface Chemistry and Morphology

17 It was shown that the surface chemistry of the electrocatalysts plays a crucial role in the
18 electrocatalytic activity and the mechanisms that are taking place [88,89]. Therefore, XPS was
19 used to identify the surface composition. The acquired full survey scans provided in [Figure S2](#)
20 indicate the prevalence of carbon, nitrogen and oxygen as major constituents where silicon is
21 present as an impurity element. In the metal functionalized samples i.e. L_Mn, L_Fe and L_FeMn
22 tiny peaks belonging to Mn and/or Fe can be appreciated while the high-resolution 2p spectra of
23 Mn and Fe in the corresponding samples are additionally displayed in [Figure S3](#). The intensities
24 of both Mn2p and Fe2p spectra came out to be very low and thus agreed with the XRD findings,
25 suggesting the homogenous presence of metallic content in traces. Li and coworkers also
26 experienced such kind of structure while developing trace bimetallic ORR electrocatalysts [51].
27 [Table S1](#) summarizes the elemental composition as well as the relative proportion of the nitrogen-
28 based species present in the samples.

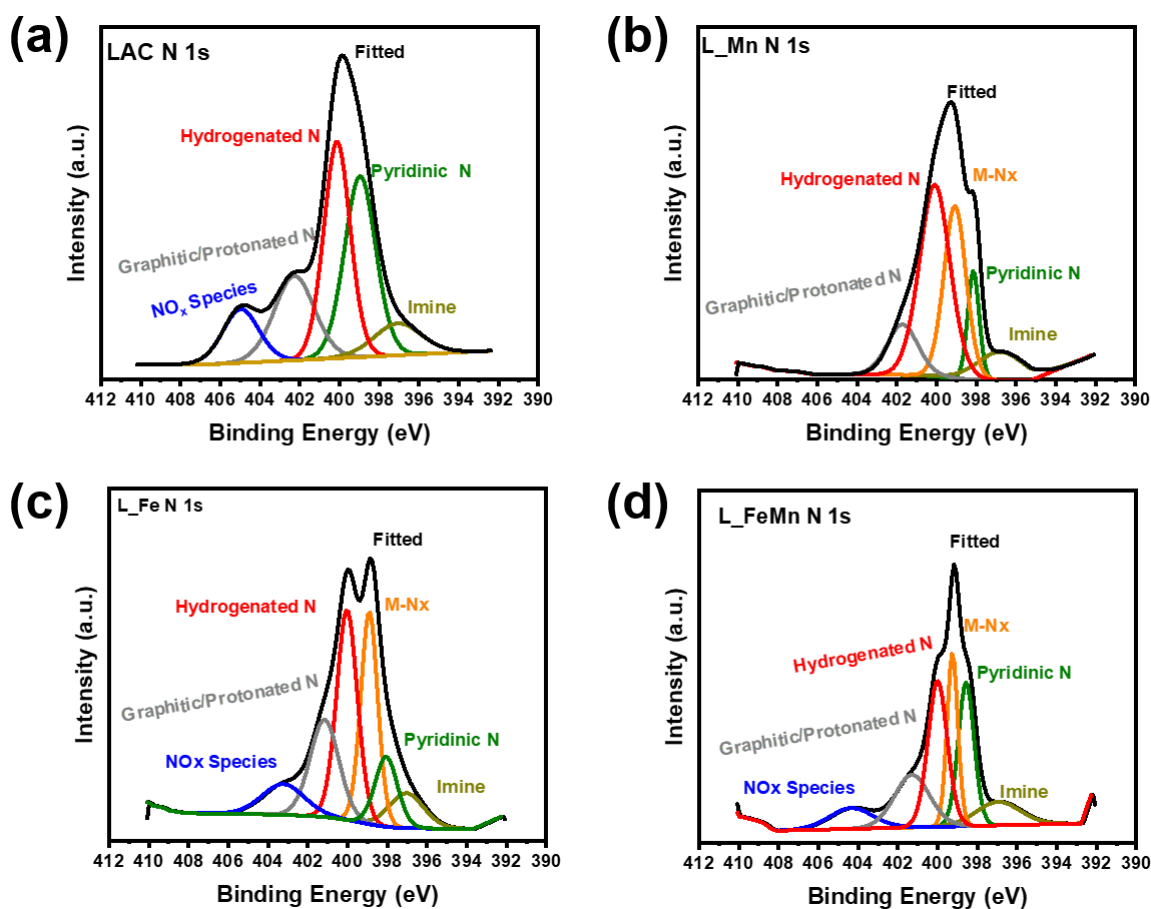
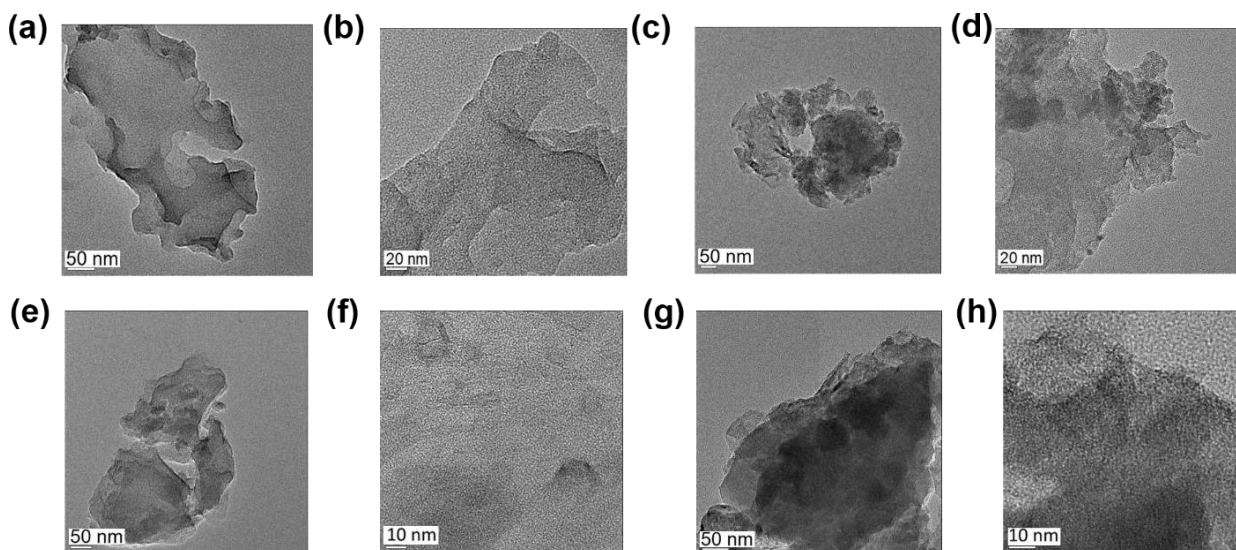


Figure 3. XPS high-resolution N 1s spectra of the as-developed samples.

As afore discussed in detail, nitrogen is an important ingredient of M-N-Cs and helps in specifying the route of ORR, N 1s high-resolution spectra of the derived samples (Figure 3) were thoroughly analyzed. Deconvolution of N 1s peak of LAC indicated the occurrence of various nitrogen species such as imine N, pyridinic N, hydrogenated N, graphitic/protonated N, and NO_x , emerging in the vicinity of their typical binding energies [21,90–95]. Interestingly the metal functionalized sample also demonstrated the presence of M-N_x . Whereas pyridinic N (0.5 at.%) was maximum in LAC with a total nitrogen content of 1.87 at.%. Nitrogen came out to be the highest in L_Fe (3.4 at.%) with the predominance of M-N_x , hydrogenated N-H and graphitic N whereas pyridinic N remained 0.36-38 at.% in all three metal functionalized samples. It is worth mentioning that the co-occurrence of various active sites can be advantageous since each of them performs particular tasks during ORR [52]. Generally, pyridinic N is considered essential for completing the electro-reduction of oxygen, especially as a secondary active site [21]. However,

1 Okada et al. also experienced superior activity of graphitic N owing to lower defect density [96].
2 Lai et al experienced the dependency of limiting current density on graphitic N while pyridine N
3 predicted the onset potential [97]. On the other hand, Kabir et al. revealed that hydrogenated N
4 (including pyrrolic and Pyridinic N-H) not only uplifts the reaction kinetics but also acts as key
5 active sites for the 2+2 e- transfer mechanism ORR in both alkaline and acidic media while
6 pyridinic N being secondary active site can be helpful in further reducing the peroxide in the
7 alkaline environment [94]. In addition to metal-free nitrogen-based moieties, M-N_x is expected to
8 carry out the direct tetra-electronic reduction of oxygen into water [98]. Moreover, the reactivity
9 of such active sites is also governed by the nature of the electrolyte to which they are exposed and
10 their roles alter as the pH of the electrolyte changes [35]. Shifting from acidic to alkaline conditions
11 switches pyridinic N-H to deprotonated pyridinic N⁻ which is a preferential adsorption site for O₂
12 due to enhanced Lewis basicity [35,99].



13 **Figure 4.** TEM images of LAC (a, b), L_Mn (c, d), L_Fe (e, f) and L_FeMn (g, h).

14
15
16 The morphological features of the derived samples were studied by the means of TEM.
17 Obtained micrographs are illustrated in Figure 4. LAC demonstrated a well-developed porous
18 structure. Such aspects of the microstructure were sustained in the MPC functionalized samples as
19 well. Microstructural features could be relatable to the outcomes of Raman spectroscopy and XRD
20 that highlighted the presence of structural defects and disorders. In a high-resolution image of
21 L_Fe (Figure 4f) a few broken graphitic domains could be appreciated. Interestingly, TEM
22 micrographs of functionalized electrocatalysts didn't show substantial agglomeration or

1
2
3
4 1 nanoparticle formation of metallic species which further validates the impression of atomically
5
6 2 dispersed metallic moieties in a homogenous fashion [100]. EDS presented in Figure S4 further
7
8 3 confirms the elements of interest i.e. Fe and Mn in the corresponding samples whereas peaks of
9
10 4 Cu belong to the TEM sample holder and Si is an impurity artifact.
11
12 5

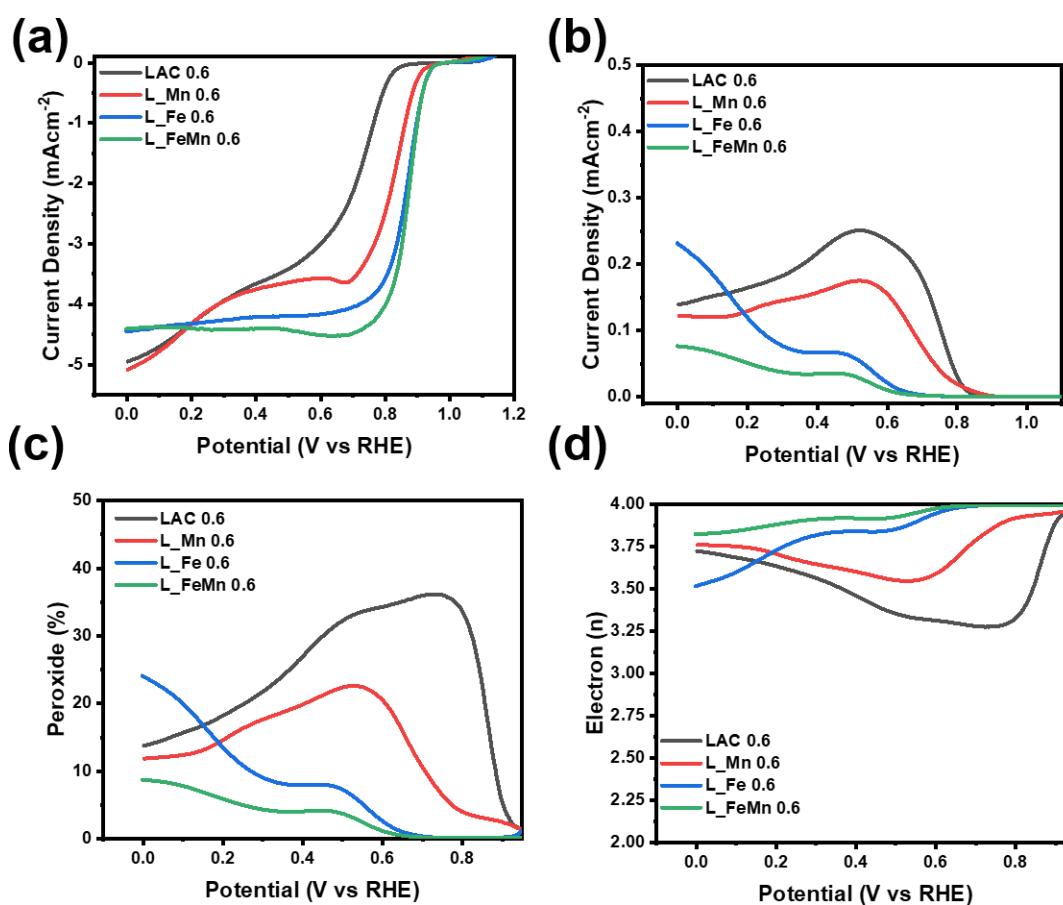
13 6 **3.4 Electrochemical Activity**

14
15 7 To elucidate the electrocatalytic aptitude of the developed electrocatalysts, RRDE measurements
16
17 8 were carried out. Changing the nature of working electrolytes not only modifies the reaction
18
19 9 mechanism but different active sites respond to ORR activity differently [101,102]. For that
20
21 10 reason, ORR measurements were obtained in alkaline and acidic media, to ensure the utility of the
22
23 11 developed electrocatalyst for AEMFC and PEMFCs, respectively. Onset potential (E_{onset}), half-
24
25 12 wave potential ($E_{1/2}$) and limiting current density (I_{limit}) are the common performance indicator
26
27 13 acquired from RRDE while the electrocatalyst loading on the disk of RRDE may affect the
28
29 14 peroxide formation. Therefore, two different loadings of 0.2 mg cm^{-2} and 0.6 mg cm^{-2} were
30
31 15 individually utilized to analyze the electrochemical aspects of the studied electrocatalysts.
32
33 16

34 17 **3.3.1 ORR Performance in Alkaline Media**

35 18 Figure 5 demonstrates the ORR activity in O_2 -saturated 0.1 M KOH with electrocatalysts loading
36
37 19 of 0.6 mg cm^{-2} while the performance with one-third loading is additionally presented in
38
39 20 Supplementary Figure S5. Polarization curves attained at a 5 mV s^{-1} scan rate highlighted the active
40
41 21 nature of the developed electrocatalysts, however, the pristine LAC came out to be the least
42
43 22 efficient with a higher overpotential. Remarkably, the functionalization of LAC with MPc
44
45 23 categorically improved the kinetics. Among all the counterparts, L_Fe and L_FeMn exhibited the
46
47 24 highest E_{onset} of $\sim 0.94 \text{ V}$ (vs RHE) with an outstanding $E_{1/2}$ of 0.87 V (vs RHE). I_{limit} remained
48
49 25 maximum for L_FeMn. LAC and L_Mn showed $E_{1/2}$ of $\sim 0.75 \text{ V}$ (vs RHE) and 0.85 V (vs RHE)
50
51 26 respectively, with 0.6 mg cm^{-2} catalyst loadings. Peroxide production showed interesting trends
52
53 27 where the electrocatalyst loading also contributed to diminishing the yield of unwanted OH_2^- . A
54
55 28 threefold increment in the electrocatalyst loading resulted in a slight positive shift of the $E_{1/2}$ along
56
57 29 with a subsequent drop in the peroxide yield. Actually, with higher loading, the produced peroxide
58
59 30 gets scavenged and then reduced within the denser layer of the electrocatalyst [103–106]. LAC
60
61 31 and L_Mn initially came out to be peroxide-producing electrocatalysts at lower overpotential
62
63
64
65

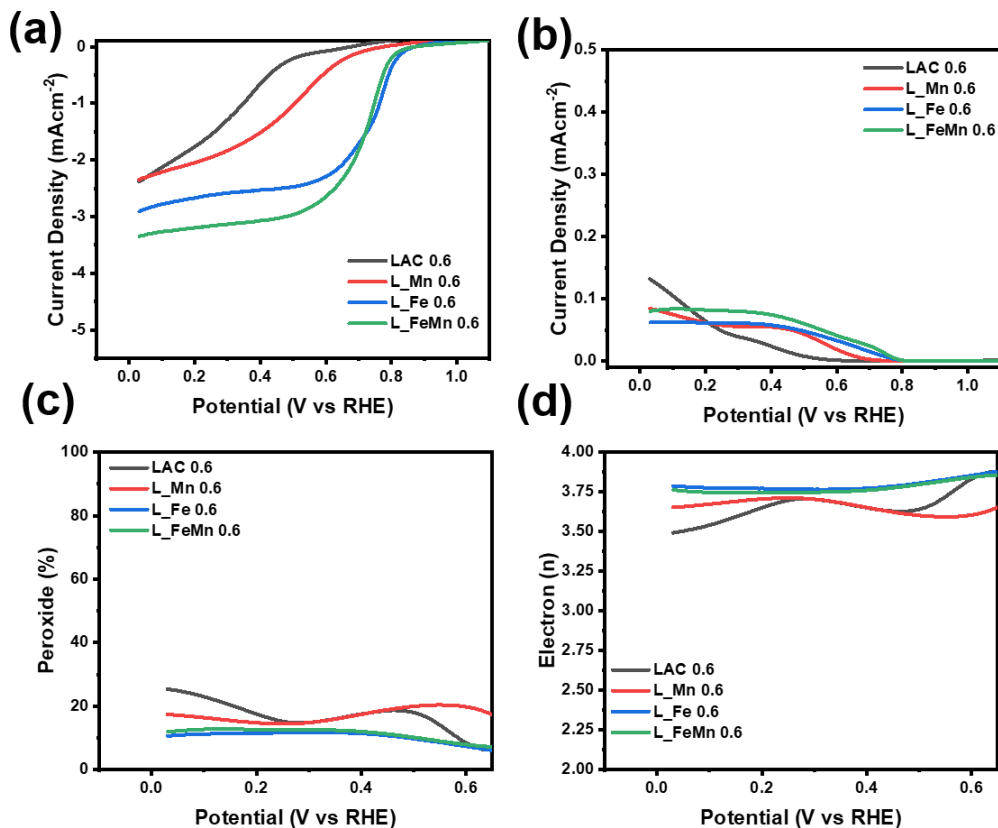
1 however a definite decline in the peroxide production can be seen as the applied potential increases.
 2 This speculation endorses the probability of a 2+2 electrons reduction pathway where the
 3 generated peroxide is afterward reduced at the secondary sites. On the other hand, L_Fe and
 4 L_FeMn tended to restrict the peroxide formation in a nearly tetra-electronic fashion. In the case
 5 of L_FeMn, peroxide yield remained confined to a maximum of ~16% and 8.7% while the electron
 6 transfer number was above 3.68 and 3.83 with 0.2 and 0.6 mg cm⁻² loading, respectively. Overall
 7 superior electrocatalytic activity is essentially credited to the dual-doping of Fe and Mn due to
 8 which electro-reduction of oxygen was synergistically boosted [40,50–52].



10
 11 **Figure 5.** RRDE measurements of the developed electrocatalysts in O₂-saturated 0.1 M KOH at
 12 1600 rpm with electrocatalyst loading of 0.6 mg cm⁻². ORR LSVs obtained at 5 mV s⁻¹ (a), ring
 13 current densities (b), peroxide yield (c) and the number of electrons (d) transferred during ORR.

15 3.3.2 ORR Performance in Acid Media

1 The efficacy of the developed electrocatalysts was additionally probed in acidic conditions
 2 comprising O₂-rich 0.5 M H₂SO₄, again using two different loadings of 0.6 mg cm⁻² (Figure 6) and
 3 0.2 mg cm⁻² (Figure S6). In acidic conditions, L_Fe with 0.6 mg cm⁻² loading exhibited E_{onset} and
 4 E_{1/2} at 0.84 V (vs RHE) and 0.77 V (vs RHE), respectively, while the I_{limit} came out to be relatively
 5 lower. Whereas L_FeMn with an E_{onset} of 0.82 V (vs RHE) showed the highest I_{limit}. Again L_Mn
 6 demonstrated the least activity among the MPC functionalized samples, confirming the
 7 inevitability of Fe for carrying out ORR with superior kinetics. Electron transfer number and
 8 peroxide yield remained nearly the same for both L_Fe and L_FeMn. Both yielded peroxide ~11-
 9 12% while maintaining the nearly tetra-electronic pathway where the electrons transfer came out
 10 to be above 3.75. Similar to alkaline situations, a positive influence of electrocatalyst loading on
 11 the ORR performance was observed and again higher loading not only improved the kinetics but
 12 also effectively decreased the peroxide yield.



14
 15 **Figure 6.** RRDE measurements of the developed electrocatalysts in O₂-saturated 0.5 M H₂SO₄
 16 at 1600 rpm with electrocatalyst loading of 0.6 mg cm⁻². ORR LSVs obtained at 5 mV s⁻¹ (a),

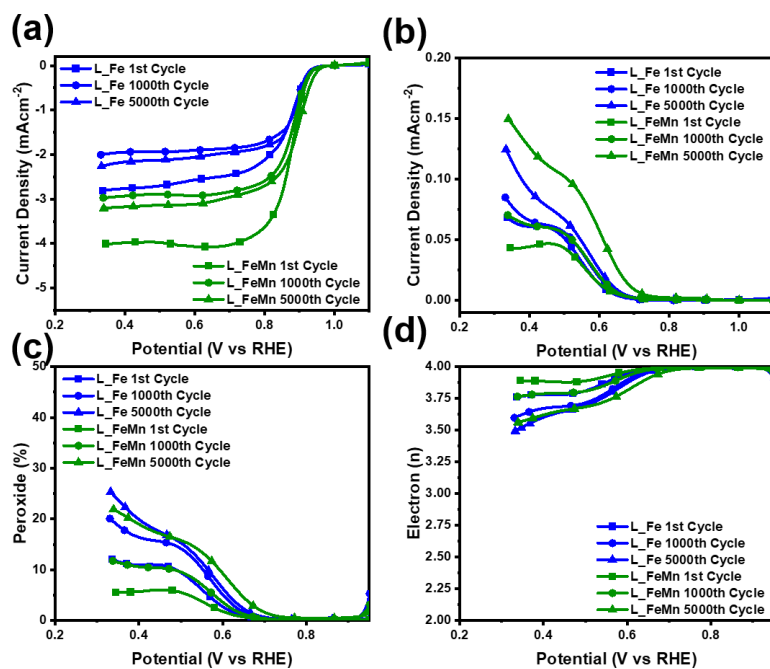
1
2
3
4 1 ring current densities (b), peroxide yield (c) and the number of electrons (d) transferred during
5
6 2 ORR
7
8 3

4 3.3.3 Electrochemical stability

11
12 5 Overall electrocatalytic activity of the L_Fe and L_FeMn turn out to be comparable where
13
14 6 L_FeMn exhibited relatively lower peroxide yield, particularly in alkaline media. While
15
16 7 comparing different sorts of monometallic and bimetallic M-N-Cs, Lilloja et al. also experienced
17
18 8 the best performance exhibited by Fe-containing monometallic and FeMn bimetallic
19
20 9 electrocatalysts [52]. Electrocatalytic activity of L_Fe and L_FeMn could be attributed to
21
22 10 structural defects as revealed by Raman, porous carbonaceous architecture visible in TEM
23
24 11 micrograph along with the coexistence of different nitrogen moieties confirmed by XPS.
25
26 12 Furthermore, microstructural analysis negated the possible agglomeration or nanoparticle
27
28 13 formation of metallic species in both samples and endorsed the homogeneous distribution at the
29
30 14 atomic level. Moreover, lower production of peroxide with satisfactory kinetics of L_FeMn can
31
32 15 be accredited to the synergic effect of Fe and Mn [40,41,50–52].

33 16 Along with favorable kinetics and desired selectivity, operational durability is an essential criterion
34
35 17 to be fulfilled by the electrocatalysts. For this reason, accelerated stability tests for L_Fe and
36
37 18 L_FeMn have been performed over 5000 continuous cycles at 50 mV s⁻¹. From **Figure 7**, in an
38
39 19 alkaline environment, reasonable stability of E_{1/2} for both electrocatalysts can be acknowledged,
40
41 20 however, a negative shift in I_{limit} can be clearly seen. At the potential of 0.4 V, I_{limit} of L_Fe was
42
43 21 diminished by 0.59 mA cm⁻² while I_{limit} of L_FeMn was lowered from 3.97 to 3.17 mA cm⁻² by
44
45 22 the 5000th cycle but still remained categorically higher than that of L_Fe. The obvious impact of
46
47 23 this observation can be speculated on the peroxide yield and the number of electrons transferred
48
49 24 during ORR. In the case of L_Fe, peroxide production was increased from 10.1% to 20.12%
50
51 25 whereas in L_FeMn the undesirable increment in peroxide was restricted to 18.5% at 0.4 V.
52
53 26 However, both electrocatalysts demonstrated nearly tetra-electronic reduction of oxygen where
54
55 27 electron transfer number persisted above 3.5. Overall, the durability aspects of both
56
57 28 electrocatalysts remained more or less the same however, L_FeMn demonstrated a relatively
58
59 29 higher I_{limit} and slightly lesser uplift in the yield of peroxide over continuous cycling. The
60
61 30 satisfactory robustness of L_FeMn encouraged the execution of stability measurements
62
63 31 additionally in the acidic conditions i.e. O₂-saturated 0.5 M H₂SO₄ and achieved trends are
64
65

1 illustrated in Figure S7. In the acidic electrolyte, the electrocatalyst didn't exhibit appreciable
 2 durability where both $E_{1/2}$ and I_{limit} were considerably affected as the cycles proceeded. By the end
 3 of the stability test, L_FeMn was left with insufficient electrocatalytic activity. The instability of
 4 PGM-free electrocatalysts in electrocatalytic media is known and there could be various complex
 5 factors damaging the durability including demetalation, deterioration of active moieties, carbon
 6 oxidation and so on [107,108]. However, analyzing the exact mechanism behind the limited
 7 stability in acidic conditions is somehow beyond the scope of the current study.



8
 9 **Figure 7.** Illustrates the stability trends of the 5000 cycles in O₂-saturated 0.1 M KOH with 0.6
 10 mg cm⁻² loading of L_Fe and L_FeMn on RRDE. ORR LSVs obtained at 5 mV s⁻¹ (a), ring
 11 current densities (b), peroxide yield (c) and the number of electrons (d) transferred during ORR
 12

13 4. Fuel Cell Testing

14
15
16
17
18
19
20
21
22
23
24
25
26
27
28
29
30
31
32
33
34
35
36
37
38
39
40
41
42
43
44
45
46
47
48
49
50
51
52
53
54
55
56
57
58
59
60
61
62
63
64
65

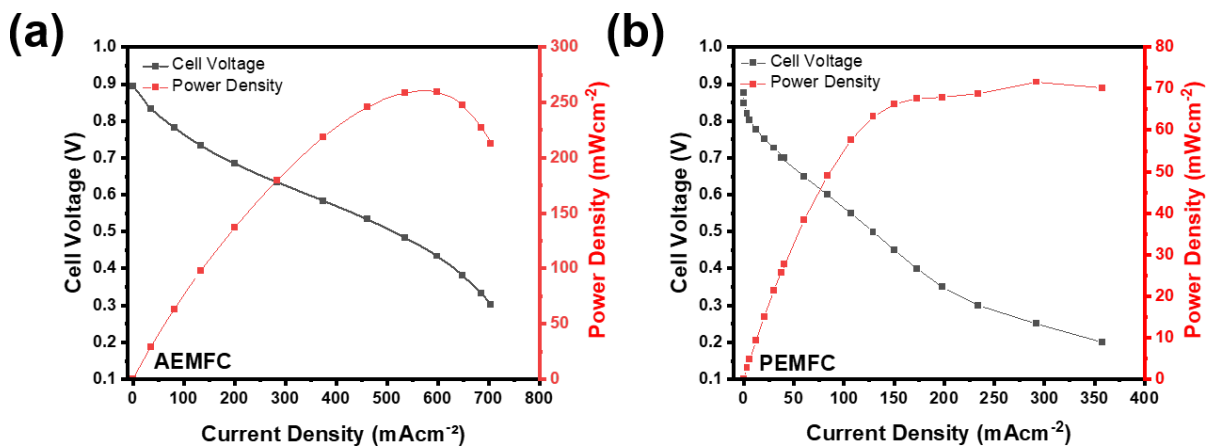


Figure 8. Full device characterization using L_FeMn as cathode electrocatalyst to perform ORR in (a) AEMFC and (b) PEMFC.

Owing to appreciable electro-kinetics and stability demonstrated by L_FeMn during the RRDE measurements, the sample was finally configured as a cathode catalyst to perform ORR in the running FCs. Full device characterizations were implemented to affirm the practicality of L_FeMn for cathode applications in both AEMFC and PEMFC. From Figure 8a, the performance of AEMFC configured with L_FeMn containing cathode can be acknowledged. AEMFC operating with a feed of pure O₂ (0.6 L min⁻¹) at 60 °C delivered an open circuit voltage (OCV) of 0.893 V. A peak power density (P_{max}) of 261 mW cm⁻² was observed at the current density of ~577 mA cm⁻². On the other hand, when L_FeMn was integrated as an ORR electrocatalyst in the cathodic configuration of PEMFC the performance was not as good as that of AEMFC, indicating that these electrocatalysts can be better employed in the alkaline environment rather than acidic environment. PEMFC was assembled with NR-211 Nafion membrane where the air was fed at the cathode operating at 80 °C. As can be seen in Figure 8b, PEMFC exhibited OCV of 0.88 V with P_{max} of ~72 mW cm⁻² at the current density of ~292 mA cm⁻².

Reasonable outcomes in AEMFC are consistent with the outstanding ORR activity of L_FeMn in the alkaline media during the half-cell testing, confirming the utility of waste biomass-derived electrocatalysts for FC applications. In spite of the fact that a true comparison with previously reported results is a bit difficult task due to variations in the designing parameters of materials and operating conditions [109–111], the obtained AEMFC performance with L_FeMn is comparable to some earlier reports. Very recently, Teppor and coworkers utilized decomposed peat as a carbon

1 precursor for synthesizing PGM-free ORR electrocatalyst and obtained P_{\max} of 51 mW cm^{-2} when
2 deployed as a cathode catalyst in AEMFC [112]. Not long ago, Lilloja et al. reported Fe–N–C
3 electrocatalyst prepared using VariPore™ method by Pajarito Powder which demonstrated P_{\max} of
4 220 mW cm^{-2} when applied in AEMFC containing HMT-PMBI membrane [113]. Similarly, Hao
5 et al. prepared multiple metals and heteroatom self-doped biomass-derived electrocatalyst which
6 performed outstandingly during the half-cell analyses in both acidic and alkaline media, however,
7 while used as an air-breathing PEMFC cathode it delivered 17.6 mW cm^{-2} with an OCV of 0.966
8 V [114]. Moreover, by the virtue of high-temperature pyrolysis, Lilloja et al. produced various
9 monometallic and bimetallic M-N-C for ORR activity in AEMFCs. They observed identical
10 behavior of monometallic Fe-N-MPC and bimetallic FeMn-N-MPC during the RRDE
11 measurements together with outstanding P_{\max} of 473 and 474 mW cm^{-2} , respectively, in AEMFC.
12 Although our full device performances are still inferior to what could be obtained using state-of-
13 the-art electrocatalysts as indicated in the literature [110,115–123], the usage of waste biomass for
14 the fabrication of cost-effective and efficient electrocatalysts presents a novel pathway under the
15 framework of the circular economy. Despite the promising performance of advanced ORR
16 electrocatalysts, their realistic employment for mass-scale FC applications is limited due to the
17 involvement of the high cost and synthetic complexity of carbon-based materials i.e. carbon
18 nanotubes and graphene-based materials [124]. Whereas the pyrolysis of largely available waste
19 biomass not only provides a sustainable alternative for the cost-effective development of carbon-
20 based electrocatalysts for green energy storage applications but also presents an effective strategy
21 for waste recycling and environmental safety.

22 23 **5. Conclusion**

24 Lignin, being waste biomass of negligible economical worth, was used to first produce activated
25 char containing networked porosity. Afterward, it was functionalized with FePc and MnPc through
26 a simplistic pyrolysis process in order to fabricate monometallic and bimetallic electrocatalysts.
27 The developed electrocatalysts demonstrated defect-rich porous structures without any
28 substitutional agglomeration in the form of metallic nanoparticles. XPS confirmed the presence of
29 a variety of nitrogen-containing active moieties. RRDE measurements in both alkaline and acidic
30 media with two different loading of 0.2 mg cm^{-2} and 0.6 mg cm^{-2} validated the active nature of the
31 derived electrocatalysts. In alkaline media, L_Fe and L_FeMn showed outstanding E_{onset} of ~ 0.942

1
2
3
4 1 V together with an $E_{1/2}$ of 0.874 V which surpasses the kinetic attributes shown by the benchmark
5
6 2 Pt/C electrocatalysts. L_FeMn showed decidedly lower peroxide yield with a clear tetra-electronic
7
8 3 electro-reduction of O_2 in 0.1 M KOH and also qualified for operational stability. Electrocatalytic
9
10 4 performance L_Fe can be linked to the favorable morphological attributes and coexistence of
11
12 5 desired nitrogen moieties. While the subsequent reduction in peroxide yield could be additionally
13
14 6 attributed synergistic of Fe and Mn. On the other hand, under acidic conditions, L_FeMn had a
15
16 7 slightly lower E_{onset} (0.817 V) than that of L_Fe (0.837 V). Contrary to 0.1 M KOH, the durability
17
18 8 of L_FeMn was severely affected in 0.5M H_2SO_4 over the 5000 cycles. Finally, to affirm the
19
20 9 realistic utility of L_FeMn for ORR in FCs it was configured as cathode electrocatalysts in both
21
22 10 PEMFC and AEMFC which delivered P_{max} of $\sim 72 \text{ mW cm}^{-2}$ (at 292 mA cm^{-2}) and 261 mW cm^{-2}
23
24 11 (at $\sim 577 \text{ mA cm}^{-2}$), respectively. Last but not the least, this works signposts the new avenues for
25
26 12 the cost-effective development of waste-derived M-N-Cs for lethargic ORR in a circular way.
27
28 13

28 14 **Acknowledgments**

29
30
31 15 C.S. would like to thank the support from the Italian Ministry of Education, Universities and
32
33 16 Research (Ministero dell'Istruzione, dell'Università e della Ricerca – MIUR) through the “Rita
34
35 17 Levi Montalcini 2018” fellowship (Grant number PGR18MAZLI). The authors also thank the
36
37 18 Italian ministry MIUR for funding through the FISR 2019 project AMPERE (FISR2019_01294).
38
39 19 University of Bologna authors acknowledge MUR support under the project “ECOSYSTEM FOR
40
41 20 SUSTAINABLE TRANSITION IN EMILIA-ROMAGNA” of the National Recovery and
42
43 21 Resilience Plan (NRRP)
44

45 22 **References**

- 46
47 23
48
49 24 [1] H. Zhang, H. Osgood, X. Xie, Y. Shao, G. Wu, Engineering nanostructures of PGM-free oxygen-
50 25 reduction catalysts using metal-organic frameworks, *Nano Energy*. 31 (2017) 331–350.
51 26 <https://doi.org/10.1016/j.nanoen.2016.11.033>.
52 27 [2] M.K. Debe, Electrocatalyst approaches and challenges for automotive fuel cells, *Nature*. 486 (2012)
53 28 43–51. <https://doi.org/10.1038/nature11115>.
54 29 [3] Y. He, S. Liu, C. Priest, Q. Shi, G. Wu, Atomically dispersed metal–nitrogen–carbon catalysts for
55 30 fuel cells: advances in catalyst design, electrode performance, and durability improvement, *Chem.*
56 31 *Soc. Rev.* 49 (2020) 3484–3524. <https://doi.org/10.1039/C9CS00903E>.
57 32 [4] N. Ramaswamy, S. Mukerjee, Fundamental Mechanistic Understanding of Electrocatalysis of
58 33 Oxygen Reduction on Pt and Non-Pt Surfaces: Acid versus Alkaline Media, *Advances in Physical*
59 34 *Chemistry*. 2012 (2012). <https://doi.org/10.1155/2012/491604>.
60
61
62
63
64
65

- 1
2
3
4 1 [5] Y. Nie, L. Li, Z. Wei, Recent advancements in Pt and Pt-free catalysts for oxygen reduction
5 2 reaction, *Chem. Soc. Rev.* 44 (2015) 2168–2201. <https://doi.org/10.1039/C4CS00484A>.
6 3 [6] R. Ma, G. Lin, Y. Zhou, Q. Liu, T. Zhang, G. Shan, M. Yang, J. Wang, A review of oxygen
7 4 reduction mechanisms for metal-free carbon-based electrocatalysts, *Npj Comput Mater.* 5 (2019) 1–
8 5 15. <https://doi.org/10.1038/s41524-019-0210-3>.
9 6 [7] A. Muthukrishnan, Y. Nabaie, T. Ohsaka, Role of iron in the reduction of H₂O₂ intermediate during
10 7 the oxygen reduction reaction on iron-containing polyimide-based electrocatalysts, *RSC Adv.* 6
11 8 (2016) 3774–3777. <https://doi.org/10.1039/C5RA23162K>.
12 9 [8] X. Zhao, Y. Liu, Origin of Selective Production of Hydrogen Peroxide by Electrochemical Oxygen
13 10 Reduction, *J. Am. Chem. Soc.* 143 (2021) 9423–9428. <https://doi.org/10.1021/jacs.1c02186>.
14 11 [9] J. Huang, Q. Lu, X. Ma, X. Yang, Bio-inspired FeN₅ moieties anchored on a three-dimensional
15 12 graphene aerogel to improve oxygen reduction catalytic performance, *J. Mater. Chem. A.* 6 (2018)
16 13 18488–18497. <https://doi.org/10.1039/C8TA06455E>.
17 14 [10] S. Guo, S. Zhang, S. Sun, Tuning Nanoparticle Catalysis for the Oxygen Reduction Reaction,
18 15 *Angewandte Chemie International Edition.* 52 (2013) 8526–8544.
19 16 <https://doi.org/10.1002/anie.201207186>.
20 17 [11] U. Tylus, Q. Jia, H. Hafiz, R.J. Allen, B. Barbiellini, A. Bansil, S. Mukerjee, Engendering anion
21 18 immunity in oxygen consuming cathodes based on Fe-N_x electrocatalysts: Spectroscopic and
22 19 electrochemical advanced characterizations, *Applied Catalysis B: Environmental.* 198 (2016) 318–
23 20 324. <https://doi.org/10.1016/j.apcatb.2016.05.054>.
24 21 [12] Y. He, Q. Tan, L. Lu, J. Sokolowski, G. Wu, Metal-Nitrogen-Carbon Catalysts for Oxygen
25 22 Reduction in PEM Fuel Cells: Self-Template Synthesis Approach to Enhancing Catalytic Activity
26 23 and Stability, *Electrochemical Energy Reviews.* 2 (2019). <https://doi.org/10.1007/s41918-019-00031-9>.
27 24 [13] S. Specchia, P. Atanassov, J.H. Zagal, Mapping transition metal–nitrogen–carbon
28 25 catalyst performance on the critical descriptor diagram, *Current Opinion in Electrochemistry.* 27
29 26 (2021) 100687. <https://doi.org/10.1016/j.coelec.2021.100687>.
30 27 [14] M. Shen, C. Wei, K. Ai, L. Lu, Transition metal–nitrogen–carbon nanostructured catalysts for the
31 28 oxygen reduction reaction: From mechanistic insights to structural optimization, *Nano Res.* 10
32 29 (2017) 1449–1470. <https://doi.org/10.1007/s12274-016-1400-7>.
33 30 [15] M.-X. Chen, L. Tong, H.-W. Liang, Understanding the Catalytic Sites of Metal–Nitrogen–Carbon
34 31 Oxygen Reduction Electrocatalysts, *Chemistry – A European Journal.* 27 (2021) 145–157.
35 32 <https://doi.org/10.1002/chem.202002427>.
36 33 [16] K. Singh, F. (Sanaz) Razmjooei, J.-S. Yu, Active sites and factors influencing them for efficient
37 34 oxygen reduction reaction in metal-N coordinated pyrolyzed and non-pyrolyzed catalysts: A review,
38 35 *J. Mater. Chem. A.* 5 (2017). <https://doi.org/10.1039/C7TA05222G>.
39 36 [17] C. Liu, H. Li, F. Liu, J. Chen, Z. Yu, Z. Yuan, C. Wang, H. Zheng, G. Henkelman, L. Wei, Y. Chen,
40 37 Intrinsic Activity of Metal Centers in Metal–Nitrogen–Carbon Single-Atom Catalysts for Hydrogen
41 38 Peroxide Synthesis, *J. Am. Chem. Soc.* 142 (2020) 21861–21871.
42 39 <https://doi.org/10.1021/jacs.0c10636>.
43 40 [18] P. Trogadas, T. Fuller, P. Strasser, Carbon as catalyst and support for electrochemical energy
44 41 conversion, *Carbon.* 75 (2014) 5–42. <https://doi.org/10.1016/j.carbon.2014.04.005>.
45 42 [19] D. Yan, Y. Li, J. Huo, R. Chen, L. Dai, S. Wang, Defect Chemistry of Nonprecious-Metal
46 43 Electrocatalysts for Oxygen Reactions, *Advanced Materials.* 29 (2017) 1606459.
47 44 <https://doi.org/10.1002/adma.201606459>.
48 45 [20] J. He, T. Zheng, D. Wu, S. Zhang, M. Gu, Q. He, Insights into the Determining Effect of Carbon
49 46 Support Properties on Anchoring Active Sites in Fe–N–C Catalysts toward the Oxygen Reduction
50 47 Reaction, *ACS Catal.* 12 (2022) 1601–1613. <https://doi.org/10.1021/acscatal.1c04815>.
51 48 [21] L. Yang, J. Shui, L. Du, Y. Shao, J. Liu, L. Dai, Z. Hu, Carbon-Based Metal-Free ORR
52 49 Electrocatalysts for Fuel Cells: Past, Present, and Future, *Advanced Materials.* 31 (2019) 1804799.
53 50 <https://doi.org/10.1002/adma.201804799>.
54 51
55
56
57
58
59
60
61
62
63
64
65

- 1
2
3
4 1 [22] O.L. Li, K. Prabakar, A. Kaneko, H. Park, T. Ishizaki, Exploration of Lewis basicity and oxygen
5 2 reduction reaction activity in plasma-tailored nitrogen-doped carbon electrocatalysts, *Catalysis*
6 3 *Today*. 337 (2019). <https://doi.org/10.1016/j.cattod.2019.02.058>.
7 4 [23] E. Berretti, M. Longhi, P. Atanassov, D. Sebastián, C. Lo Vecchio, V. Baglio, A. Serov, A.
8 5 Marchionni, F. Vizza, C. Santoro, A. Lavacchi, Platinum group metal-free Fe-based (FeNC) oxygen
9 6 reduction electrocatalysts for direct alcohol fuel cells, *Current Opinion in Electrochemistry*. 29
10 7 (2021) 100756. <https://doi.org/10.1016/j.coelec.2021.100756>.
11 8 [24] C.Z. Loyola, S. Ureta-Zañartu, J.H. Zagal, F. Tasca, Activity volcano plots for the oxygen reduction
12 9 reaction using FeN₄ complexes: From reported experimental data to the electrochemical meaning,
13 10 *Current Opinion in Electrochemistry*. 32 (2022) 100923.
14 11 <https://doi.org/10.1016/j.coelec.2021.100923>.
15 12 [25] K. Ozoemena, Nanostructured platinum-free electrocatalysts in alkaline direct alcohol fuel cells:
16 13 Catalyst design, principles and applications, *RSC Adv.* 6 (2016).
17 14 <https://doi.org/10.1039/C6RA15057H>.
18 15 [26] J.H. Zagal, I. Ponce, R. Oñate, Redox Potentials as Reactivity Descriptors in Electrochemistry,
19 16 IntechOpen, 2019. <https://doi.org/10.5772/intechopen.89883>.
20 17 [27] U. Tylus, Q. Jia, K. Strickland, N. Ramaswamy, A. Serov, P. Atanassov, S. Mukerjee, Elucidating
21 18 Oxygen Reduction Active Sites in Pyrolyzed Metal–Nitrogen Coordinated Non-Precious-Metal
22 19 Electrocatalyst Systems, *J. Phys. Chem. C*. 118 (2014) 8999–9008.
23 20 <https://doi.org/10.1021/jp500781v>.
24 21 [28] R. Venegas, F.J. Recio, J. Riquelme, K. Neira, J.F. Marco, I. Ponce, J.H. Zagal, F. Tasca,
25 22 Biomimetic reduction of O₂ in an acid medium on iron phthalocyanines axially coordinated to
26 23 pyridine anchored on carbon nanotubes, *J. Mater. Chem. A*. 5 (2017) 12054–12059.
27 24 <https://doi.org/10.1039/C7TA02381B>.
28 25 [29] A. Kozhushner, N. Zion, L. Elbaz, Methods for assessment and measurement of the active site
29 26 density in platinum group metal–free oxygen reduction reaction catalysts, *Current Opinion in*
30 27 *Electrochemistry*. 25 (2021) 100620. <https://doi.org/10.1016/j.coelec.2020.08.002>.
31 28 [30] Q. Jia, N. Ramaswamy, U. Tylus, K. Strickland, J. Li, A. Serov, K. Artyushkova, P. Atanassov, J.
32 29 Anibal, C. Gumeci, S.C. Barton, M.-T. Sougrati, F. Jaouen, B. Halevi, S. Mukerjee, Spectroscopic
33 30 insights into the nature of active sites in iron–nitrogen–carbon electrocatalysts for oxygen reduction
34 31 in acid, *Nano Energy*. 29 (2016) 65–82. <https://doi.org/10.1016/j.nanoen.2016.03.025>.
35 32 [31] J.H. Zagal, S. Griveau, J.F. Silva, T. Nyokong, F. Bedioui, Metallophthalocyanine-based molecular
36 33 materials as catalysts for electrochemical reactions, *Coordination Chemistry Reviews*. 254 (2010)
37 34 2755–2791. <https://doi.org/10.1016/j.ccr.2010.05.001>.
38 35 [32] J. Zagal, M. Páez, A.A. Tanaka, J.R. dos Santos, C.A. Linkous, Electrocatalytic activity of metal
39 36 phthalocyanines for oxygen reduction, *Journal of Electroanalytical Chemistry*. 339 (1992) 13–30.
40 37 [https://doi.org/10.1016/0022-0728\(92\)80442-7](https://doi.org/10.1016/0022-0728(92)80442-7).
41 38 [33] T. Marshall-Roth, N.J. Libretto, A.T. Wrobel, K.J. Anderton, M.L. Pegis, N.D. Rieke, T.V. Voorhis,
42 39 J.T. Miller, Y. Surendranath, A pyridinic Fe–N₄ macrocycle models the active sites in Fe/N-doped
43 40 carbon electrocatalysts, *Nat Commun*. 11 (2020) 5283. [https://doi.org/10.1038/s41467-020-18969-](https://doi.org/10.1038/s41467-020-18969-6)
44 41 [6](https://doi.org/10.1038/s41467-020-18969-6).
45 42 [34] X.X. Wang, M.T. Swihart, G. Wu, Achievements, challenges and perspectives on cathode catalysts
46 43 in proton exchange membrane fuel cells for transportation, *Nat Catal*. 2 (2019) 578–589.
47 44 <https://doi.org/10.1038/s41929-019-0304-9>.
48 45 [35] T. Asset, P. Atanassov, Iron-Nitrogen-Carbon Catalysts for Proton Exchange Membrane Fuel Cells,
49 46 *Joule*. 4 (2020) 33–44. <https://doi.org/10.1016/j.joule.2019.12.002>.
50 47 [36] U. Martinez, S. Komini Babu, E.F. Holby, H.T. Chung, X. Yin, P. Zelenay, Progress in the
51 48 Development of Fe-Based PGM-Free Electrocatalysts for the Oxygen Reduction Reaction,
52 49 *Advanced Materials*. 31 (2019) 1806545. <https://doi.org/10.1002/adma.201806545>.
53 50 [37] Q. Liu, Y. Wang, Z. Hu, Z. Zhang, Iron-based single-atom electrocatalysts: synthetic strategies and
54 51 applications, *RSC Adv.* 11 (2021) 3079–3095. <https://doi.org/10.1039/D0RA08223F>.
55
56
57
58
59
60
61
62
63
64
65

- 1
2
3
4 1 [38] J. Li, M.T. Sougrati, A. Zitolo, J.M. Ablett, I.C. Oğuz, T. Mineva, I. Matanovic, P. Atanassov, Y.
5 2 Huang, I. Zenyuk, A. Di Cicco, K. Kumar, L. Dubau, F. Maillard, G. Dražić, F. Jaouen,
6 3 Identification of durable and non-durable Fe_{Nx} sites in Fe–N–C materials for proton exchange
7 4 membrane fuel cells, *Nat Catal.* 4 (2021) 10–19. <https://doi.org/10.1038/s41929-020-00545-2>.
- 8 5 [39] W. Wang, Q. Jia, S. Mukerjee, S. Chen, Recent Insights into the Oxygen-Reduction Electrocatalysis
9 6 of Fe/N/C Materials, *ACS Catal.* 9 (2019) 10126–10141. <https://doi.org/10.1021/acscatal.9b02583>.
- 10 7 [40] Y. Kumar, E. Kibena-Pöldsepp, J. Kozlova, M. Rähn, A. Treshchalov, A. Kikas, V. Kisand, J.
11 8 Aruväli, A. Tamm, J.C. Douglin, S.J. Folkman, I. Gelmetti, F.A. Garcés-Pineda, J.R. Galán-
12 9 Mascarós, D.R. Dekel, K. Tammeveski, Bifunctional Oxygen Electrocatalysis on Mixed Metal
13 10 Phthalocyanine-Modified Carbon Nanotubes Prepared via Pyrolysis, *ACS Appl. Mater. Interfaces.*
14 11 13 (2021) 41507–41516. <https://doi.org/10.1021/acsami.1c06737>.
- 15 12 [41] A. Serov, M.H. Robson, M. Smolnik, P. Atanassov, Templated bi-metallic non-PGM catalysts for
16 13 oxygen reduction, *Electrochimica Acta.* 80 (2012) 213–218.
17 14 <https://doi.org/10.1016/j.electacta.2012.07.008>.
- 18 15 [42] B. Zhong, L. Zhang, J. Yu, K. Fan, Ultrafine iron-cobalt nanoparticles embedded in nitrogen-doped
19 16 porous carbon matrix for oxygen reduction reaction and zinc-air batteries, *Journal of Colloid and*
20 17 *Interface Science.* 546 (2019) 113–121. <https://doi.org/10.1016/j.jcis.2019.03.038>.
- 21 18 [43] W. Ran, J. Dong, T. Sun, J. Chen, L. Xu, Iron, Cobalt, and Nitrogen Tri-Doped Ordered
22 19 Mesoporous Carbon as a Highly Efficient Electrocatalyst for Oxygen Reduction Reaction,
23 20 *ChemistrySelect.* 4 (2019) 7728–7733. <https://doi.org/10.1002/slct.201901641>.
- 24 21 [44] W.-K. Jo, S. Moru, D.-E. Lee, S. Tonda, Cobalt- and iron-coordinated graphitic carbon nitride on
25 22 reduced graphene oxide: A nonprecious bimetallic M–N_x–C analogue electrocatalyst for efficient
26 23 oxygen reduction reaction in acidic media, *Applied Surface Science.* 531 (2020) 147367.
27 24 <https://doi.org/10.1016/j.apsusc.2020.147367>.
- 28 25 [45] Z. Hu, Z. Guo, Z. Zhang, M. Dou, F. Wang, Bimetal Zeolitic Imidazolate Framework-Derived Iron-,
29 26 Cobalt- and Nitrogen-Codoped Carbon Nanopolyhedra Electrocatalyst for Efficient Oxygen
30 27 Reduction, *ACS Appl. Mater. Interfaces.* 10 (2018) 12651–12658.
31 28 <https://doi.org/10.1021/acsami.8b00512>.
- 32 29 [46] R. Mercado, C. Wahl, J. En Lu, T. Zhang, B. Lu, P. Zhang, J.Q. Lu, A. Allen, J.Z. Zhang, S. Chen,
33 30 Nitrogen-Doped Porous Carbon Cages for Electrocatalytic Reduction of Oxygen: Enhanced
34 31 Performance with Iron and Cobalt Dual Metal Centers, *ChemCatChem.* 12 (2020) 3230–3239.
35 32 <https://doi.org/10.1002/cctc.201902324>.
- 36 33 [47] Priorities for critical materials for a circular economy, EASAC – the European Academies’ Science
37 34 Advisory Council, Halle (Saale) Germany, 2016.
- 38 35 [48] I. Directorate-General for Internal Market, S. Bobba, P. Claudiu, D. Huygens, P. Alves Dias, B.
39 36 Gawlik, E. Tzimas, D. Wittmer, P. Nuss, M. Grohol, H. Saveyn, F. Buraoui, G. Orveillon, T.
40 37 Hámor, S. Slavko, F. Mathieux, M. Gislev, C. Torres De Matos, G.A. Blengini, F. Ardente, D.
41 38 Blagoeva, E. Garbarino, Report on critical raw materials and the circular economy, Publications
42 39 Office of the European Union, LU, 2018. <https://data.europa.eu/doi/10.2873/167813> (accessed May
43 40 7, 2022).
- 44 41 [49] Y. Sun, L. Silvioli, N.R. Sahraie, W. Ju, J. Li, A. Zitolo, S. Li, A. Bagger, L. Arnarson, X. Wang, T.
45 42 Moeller, D. Bernsmeier, J. Rossmesl, F. Jaouen, P. Strasser, Activity–Selectivity Trends in the
46 43 Electrochemical Production of Hydrogen Peroxide over Single-Site Metal–Nitrogen–Carbon
47 44 Catalysts, *J. Am. Chem. Soc.* 141 (2019) 12372–12381. <https://doi.org/10.1021/jacs.9b05576>.
- 48 45 [50] M. Kodali, C. Santoro, S. Herrera, A. Serov, P. Atanassov, Bimetallic platinum group metal-free
49 46 catalysts for high power generating microbial fuel cells, *Journal of Power Sources.* 366 (2017) 18–
50 47 26. <https://doi.org/10.1016/j.jpowsour.2017.08.110>.
- 51 48 [51] F. Li, P. Shi, J. Wu, X. Qi, Y. Liu, G. Li, Trace Bimetallic Iron/Manganese Co-Doped N-
52 49 Ketjenblack Carbon Electrocatalyst for Robust Oxygen Reduction Reaction, *J. Electrochem. Soc.*
53 50 168 (2021) 060502. <https://doi.org/10.1149/1945-7111/ac03f3>.
- 54
55
56
57
58
59
60
61
62
63
64
65

- 1
2
3
4 1 [52] J. Lilloja, E. Kibena-Pöldsepp, A. Sarapuu, M. Käärrik, J. Kozlova, P. Paiste, A. Kikas, A.
5 2 Treshchalov, J. Leis, A. Tamm, V. Kisand, S. Holdcroft, K. Tammeveski, Transition metal and
6 3 nitrogen-doped mesoporous carbons as cathode catalysts for anion-exchange membrane fuel cells,
7 4 *Applied Catalysis B: Environmental*. 306 (2022) 121113.
8 5 <https://doi.org/10.1016/j.apcatb.2022.121113>.
9 6 [53] M. Borghei, J. Lehtonen, L. Liu, O.J. Rojas, *Advanced Biomass-Derived Electrocatalysts for the*
10 7 *Oxygen Reduction Reaction*, *Advanced Materials*. 30 (2018) 1703691.
11 8 <https://doi.org/10.1002/adma.201703691>.
12 9 [54] M. Wang, S. Wang, H. Yang, W. Ku, S. Yang, Z. Liu, G. Lu, Carbon-Based Electrocatalysts
13 10 Derived From Biomass for Oxygen Reduction Reaction: A Minireview, *Frontiers in Chemistry*. 8
14 11 (2020). <https://www.frontiersin.org/article/10.3389/fchem.2020.00116> (accessed May 7, 2022).
15 12 [55] L. Du, G. Zhang, X. Liu, A. Hassanpour, M. Dubois, A.C. Tavares, S. Sun, Biomass-derived
16 13 nonprecious metal catalysts for oxygen reduction reaction: The demand-oriented engineering of
17 14 active sites and structures, *Carbon Energy*. 2 (2020) 561–581. <https://doi.org/10.1002/cey2.73>.
18 15 [56] M. Jiang, X. Yu, H. Yang, S. Chen, Optimization Strategies of Preparation of Biomass-Derived
19 16 Carbon Electrocatalyst for Boosting Oxygen Reduction Reaction: A Minireview, *Catalysts*. 10
20 17 (2020) 1472. <https://doi.org/10.3390/catal10121472>.
21 18 [57] S. Zago, M. Bartoli, M. Muhyuddin, G.M. Vanacore, P. Jagdale, A. Tagliaferro, C. Santoro, S.
22 19 Specchia, Engineered biochar derived from pyrolyzed waste tea as a carbon support for Fe-N-C
23 20 electrocatalysts for the oxygen reduction reaction, *Electrochimica Acta*. 412 (2022) 140128.
24 21 <https://doi.org/10.1016/j.electacta.2022.140128>.
25 22 [58] J. Munuera, L. Britnell, C. Santoro, R. Cuéllar-Franca, C. Casiraghi, A review on sustainable
26 23 production of graphene and related life cycle assessment, *2D Mater*. 9 (2021) 012002.
27 24 <https://doi.org/10.1088/2053-1583/ac3f23>.
28 25 [59] B.K. Mutuma, N.F. Sylla, A. Bubu, N.M. Ndiaye, C. Santoro, A. Brilloni, F. Poli, N. Manyala, F.
29 26 Soavi, Valorization of biodigester plant waste in electrodes for supercapacitors and microbial fuel
30 27 cells, *Electrochimica Acta*. 391 (2021) 138960. <https://doi.org/10.1016/j.electacta.2021.138960>.
31 28 [60] M. Muhyuddin, P. Mustarelli, C. Santoro, Recent Advances in Waste Plastic Transformation into
32 29 Valuable Platinum-Group Metal-Free Electrocatalysts for Oxygen Reduction Reaction,
33 30 *ChemSusChem*. 14 (2021) 3785–3800. <https://doi.org/10.1002/cssc.202101252>.
34 31 [61] N. Cai, H. Yang, X. Zhang, S. Xia, D. Yao, P. Bartocci, F. Fantozzi, Y. Chen, H. Chen, P.T.
35 32 Williams, Bimetallic carbon nanotube encapsulated Fe-Ni catalysts from fast pyrolysis of waste
36 33 plastics and their oxygen reduction properties, *Waste Management*. 109 (2020) 119–126.
37 34 <https://doi.org/10.1016/j.wasman.2020.05.003>.
38 35 [62] N. Cai, S. Xia, X. Zhang, Z. Meng, P. Bartocci, F. Fantozzi, Y. Chen, H. Chen, P.T. Williams, H.
39 36 Yang, Preparation of Iron- and Nitrogen-Codoped Carbon Nanotubes from Waste Plastics Pyrolysis
40 37 for the Oxygen Reduction Reaction, *ChemSusChem*. 13 (2020) 938–944.
41 38 <https://doi.org/10.1002/cssc.201903293>.
42 39 [63] G. Daniel, T. Kosmala, M.C. Dalconi, L. Nodari, D. Badocco, P. Pastore, A. Lorenzetti, G.
43 40 Granozzi, C. Durante, Upcycling of polyurethane into iron-nitrogen-carbon electrocatalysts active
44 41 for oxygen reduction reaction, *Electrochimica Acta*. 362 (2020) 137200.
45 42 <https://doi.org/10.1016/j.electacta.2020.137200>.
46 43 [64] M. Muhyuddin, J. Filippi, L. Zoia, S. Bonizzoni, R. Lorenzi, E. Berretti, L. Capozzoli, M. Bellini,
47 44 C. Ferrara, A. Lavacchi, C. Santoro, Waste Face Surgical Mask Transformation into Crude Oil and
48 45 Nanostructured Electrocatalysts for Fuel Cells and Electrolyzers, *ChemSusChem*. 15 (2022)
49 46 e202102351. <https://doi.org/10.1002/cssc.202102351>.
50 47 [65] *Converting Waste Agricultural Biomass into a Resource-Compendium of Technologies*, United
51 48 Nations Environmental Programme, , Japan, 2009.
52 49 <https://wedocs.unep.org/xmlui/handle/20.500.11822/7614> (accessed May 7, 2022).
53
54
55
56
57
58
59
60
61
62
63
64
65

- 1
2
3
4 1 [66] H. Zhou, T. Fan, D. Zhang, Biotemplated Materials for Sustainable Energy and Environment:
5 2 Current Status and Challenges, *ChemSusChem*. 4 (2011) 1344–1387.
6 3 <https://doi.org/10.1002/cssc.201100048>.
7 4 [67] D.L. Klass, *Biomass for Renewable Energy, Fuels, and Chemicals*, Elsevier, 1998.
8 5 [68] M. Garedeew, F. Lin, B. Song, T.M. DeWinter, J.E. Jackson, C.M. Saffron, C.H. Lam, P.T. Anastas,
9 6 Greener Routes to Biomass Waste Valorization: Lignin Transformation Through Electrocatalysis
10 7 for Renewable Chemicals and Fuels Production, *ChemSusChem*. 13 (2020) 4214–4237.
11 8 <https://doi.org/10.1002/cssc.202000987>.
12 9 [69] H.Y. Lim, S. Yusup, A.C.M. Loy, S. Samsuri, S.S.K. Ho, A.S.A. Manaf, S.S. Lam, B.L.F. Chin,
13 10 M.N. Acda, P. Unrean, E. Rianawati, Review on Conversion of Lignin Waste into Value-Added
14 11 Resources in Tropical Countries, *Waste Biomass Valor.* 12 (2021) 5285–5302.
15 12 <https://doi.org/10.1007/s12649-020-01307-8>.
16 13 [70] D.S. Bajwa, G. Pourhashem, A.H. Ullah, S.G. Bajwa, A concise review of current lignin
17 14 production, applications, products and their environmental impact, *Industrial Crops and Products*.
18 15 139 (2019) 111526. <https://doi.org/10.1016/j.indcrop.2019.111526>.
19 16 [71] I. Haq, P. Mazumder, A.S. Kalamdhad, Recent advances in removal of lignin from paper industry
20 17 wastewater and its industrial applications – A review, *Bioresource Technology*. 312 (2020) 123636.
21 18 <https://doi.org/10.1016/j.biortech.2020.123636>.
22 19 [72] M. Bellini, M.V. Pagliaro, A. Lenarda, P. Fornasiero, M. Marelli, C. Evangelisti, M. Innocenti, Q.
23 20 Jia, S. Mukerjee, J. Jankovic, L. Wang, J.R. Varcoe, C.B. Krishnamurthy, I. Grinberg, E. Davydova,
24 21 D.R. Dekel, H.A. Miller, F. Vizza, Palladium–Ceria Catalysts with Enhanced Alkaline Hydrogen
25 22 Oxidation Activity for Anion Exchange Membrane Fuel Cells, *ACS Appl. Energy Mater.* 2 (2019)
26 23 4999–5008. <https://doi.org/10.1021/acsaem.9b00657>.
27 24 [73] H.A. Miller, M.V. Pagliaro, M. Bellini, F. Bartoli, L. Wang, I. Salam, J.R. Varcoe, F. Vizza,
28 25 Integration of a Pd-CeO₂/C Anode with Pt and Pt-Free Cathode Catalysts in High Power Density
29 26 Anion Exchange Membrane Fuel Cells, *ACS Appl. Energy Mater.* 3 (2020) 10209–10214.
30 27 <https://doi.org/10.1021/acsaem.0c01998>.
31 28 [74] L. Wang, X. Peng, W.E. Mustain, J.R. Varcoe, Radiation-grafted anion-exchange membranes: the
32 29 switch from low- to high-density polyethylene leads to remarkably enhanced fuel cell performance,
33 30 *Energy Environ. Sci.* 12 (2019) 1575–1579. <https://doi.org/10.1039/C9EE00331B>.
34 31 [75] S. Liu, L. Liu, X. Chen, Z. Yang, M. Li, Y. Wang, W. Lv, P. Zhu, X. Zhao, G. Wang, On an Easy
35 32 Way to Prepare Fe, S, N Tri-Doped Mesoporous Carbon Materials as Efficient Electrocatalysts for
36 33 Oxygen Reduction Reaction, *Electrocatalysis*. 10 (2019) 72–81. <https://doi.org/10.1007/s12678-018-0496-9>.
37 34 [76] C. Zhu, Q. Shi, B. Xu, S. Fu, G. Wan, C. Yang, S. Yao, J. Song, H. Zhou, D. Du, S. Beckman, D.
38 35 Su, Y. Lin, Hierarchically Porous M-N-C (M = Co and Fe) Single-Atom Electrocatalysts with
39 36 Robust MN_x Active Moieties Enable Enhanced ORR Performance, *Advanced Energy Materials*. 8
40 37 (2018) 1801956. <https://doi.org/10.1002/aenm.201801956>.
41 38 [77] T. Liu, F. Sun, M. Huang, L. Guan, Atomically dispersed Co–N–C electrocatalysts synthesized by a
42 39 low-speed ball milling method for proton exchange membrane fuel cells, *Materials Advances*. 3
43 40 (2022) 1565–1573. <https://doi.org/10.1039/D1MA00809A>.
44 41 [78] X. Luo, X. Wei, H. Wang, W. Gu, T. Kaneko, Y. Yoshida, X. Zhao, C. Zhu, Secondary-Atom-
45 42 Doping Enables Robust Fe–N–C Single-Atom Catalysts with Enhanced Oxygen Reduction
46 43 Reaction, *Nano-Micro Lett.* 12 (2020) 163. <https://doi.org/10.1007/s40820-020-00502-5>.
47 44 [79] C. Xin, W. Shang, J. Hu, C. Zhu, J. Guo, J. Zhang, H. Dong, W. Liu, Y. Shi, Integration of
48 45 Morphology and Electronic Structure Modulation on Atomic Iron- Nitrogen- Carbon Catalysts for
49 46 Highly Efficient Oxygen Reduction, *Advanced Functional Materials*. 32 (2022).
50 47 <https://doi.org/10.1002/adfm.202108345>.
51 48 [80] H. Yang, L. Shang, Q. Zhang, R. Shi, G. Waterhouse, L. Gu, T. Zhang, A universal ligand mediated
52 49 method for large scale synthesis of transition metal single atom catalysts, *Nature Communications*.
53 50 10 (2019) 1–9. <https://doi.org/10.1038/s41467-019-12510-0>.
54 51
55
56
57
58
59
60
61
62
63
64
65

- 1
2
3
4 1 [81] A.C. Ferrari, J. Robertson, Interpretation of Raman spectra of disordered and amorphous carbon,
5 2 Phys. Rev. B. 61 (2000) 14095–14107. <https://doi.org/10.1103/PhysRevB.61.14095>.
- 6 3 [82] L.G. Cançado, A. Jorio, E.H.M. Ferreira, F. Stavale, C.A. Achete, R.B. Capaz, M.V.O. Moutinho,
7 4 A. Lombardo, T.S. Kulmala, A.C. Ferrari, Quantifying Defects in Graphene via Raman
8 5 Spectroscopy at Different Excitation Energies, Nano Lett. 11 (2011) 3190–3196.
9 6 <https://doi.org/10.1021/nl201432g>.
- 10 7 [83] C. Casimero, C. Hegarty, R.J. McGlynn, J. Davis, Ultrasonic exfoliation of carbon fiber:
11 8 electroanalytical perspectives, J Appl Electrochem. 50 (2020) 383–394.
12 9 <https://doi.org/10.1007/s10800-019-01379-y>.
- 13 10 [84] B.J. Matsoso, K. Ranganathan, B.K. Mutuma, T. Lerotholi, G. Jones, N.J. Coville, Time-dependent
14 11 evolution of the nitrogen configurations in N-doped graphene films, RSC Adv. 6 (2016) 106914–
15 12 106920. <https://doi.org/10.1039/C6RA24094A>.
- 16 13 [85] L.M. Malard, M.A. Pimenta, G. Dresselhaus, M.S. Dresselhaus, Raman spectroscopy in graphene,
17 14 Physics Reports. 473 (2009) 51–87. <https://doi.org/10.1016/j.physrep.2009.02.003>.
- 18 15 [86] P. Song, M. Luo, X. Liu, W. Xing, W. Xu, Z. Jiang, L. Gu, Zn Single Atom Catalyst for Highly
19 16 Efficient Oxygen Reduction Reaction, Advanced Functional Materials. 27 (2017) 1700802.
20 17 <https://doi.org/10.1002/adfm.201700802>.
- 21 18 [87] J. Wang, F. Ciucci, Boosting Bifunctional Oxygen Electrolysis for N-Doped Carbon via Bimetal
22 19 Addition, Small. 13 (2017) 1604103. <https://doi.org/10.1002/smll.201604103>.
- 23 20 [88] K. Artyushkova, A. Serov, S. Rojas-Carbonell, P. Atanassov, Chemistry of Multitudinous Active
24 21 Sites for Oxygen Reduction Reaction in Transition Metal–Nitrogen–Carbon Electrocatalysts, J.
25 22 Phys. Chem. C. 119 (2015) 25917–25928. <https://doi.org/10.1021/acs.jpcc.5b07653>.
- 26 23 [89] C. Santoro, P. Bollella, B. Erable, P. Atanassov, D. Pant, Oxygen reduction reaction electrocatalysis
27 24 in neutral media for bioelectrochemical systems, Nat Catal. 5 (2022) 473–484.
28 25 <https://doi.org/10.1038/s41929-022-00787-2>.
- 29 26 [90] P. Lazar, R. Mach, M. Otyepka, Spectroscopic Fingerprints of Graphitic, Pyrrolic, Pyridinic, and
30 27 Chemisorbed Nitrogen in N-Doped Graphene, J. Phys. Chem. C. 123 (2019) 10695–10702.
31 28 <https://doi.org/10.1021/acs.jpcc.9b02163>.
- 32 29 [91] K. Artyushkova, Misconceptions in interpretation of nitrogen chemistry from x-ray
33 30 photoelectron spectra, Journal of Vacuum Science & Technology A. 38 (2020) 031002.
34 31 <https://doi.org/10.1116/1.5135923>.
- 35 32 [92] M. Kodali, C. Santoro, A. Serov, S. Kabir, K. Artyushkova, I. Matanovic, P. Atanassov, Air
36 33 Breathing Cathodes for Microbial Fuel Cell using Mn-, Fe-, Co- and Ni-containing Platinum Group
37 34 Metal-free Catalysts, Electrochimica Acta. 231 (2017) 115–124.
38 35 <https://doi.org/10.1016/j.electacta.2017.02.033>.
- 39 36 [93] M.J. Dzara, K. Artyushkova, S. Shulda, M.B. Strand, C. Ngo, E.J. Crumlin, T. Gennett, S.
40 37 Pylypenko, Characterization of Complex Interactions at the Gas–Solid Interface with in Situ
41 38 Spectroscopy: The Case of Nitrogen-Functionalized Carbon, J. Phys. Chem. C. 123 (2019) 9074–
42 39 9086. <https://doi.org/10.1021/acs.jpcc.9b00487>.
- 43 40 [94] S. Kabir, K. Artyushkova, A. Serov, P. Atanassov, Role of Nitrogen Moieties in N-Doped 3D-
44 41 Graphene Nanosheets for Oxygen Electroreduction in Acidic and Alkaline Media, ACS Appl.
45 42 Mater. Interfaces. 10 (2018) 11623–11632. <https://doi.org/10.1021/acsami.7b18651>.
- 46 43 [95] C. Santoro, S. Rojas-Carbonell, R. Awais, R. Gokhale, M. Kodali, A. Serov, K. Artyushkova, P.
47 44 Atanassov, Influence of platinum group metal-free catalyst synthesis on microbial fuel cell
48 45 performance, Journal of Power Sources. 375 (2018) 11–20.
49 46 <https://doi.org/10.1016/j.jpowsour.2017.11.039>.
- 50 47 [96] T. Okada, K.Y. Inoue, G. Kalita, M. Tanemura, T. Matsue, M. Meyyappan, S. Samukawa, Bonding
51 48 state and defects of nitrogen-doped graphene in oxygen reduction reaction, Chemical Physics
52 49 Letters. 665 (2016) 117–120. <https://doi.org/10.1016/j.cplett.2016.10.061>.
- 53
54
55
56
57
58
59
60
61
62
63
64
65

- 1
2
3
4 1 [97] L. Lai, J.R. Potts, D. Zhan, L. Wang, C.K. Poh, C. Tang, H. Gong, Z. Shen, J. Lin, R.S. Ruoff,
5 2 Exploration of the active center structure of nitrogen-doped graphene-based catalysts for oxygen
6 3 reduction reaction, *Energy Environ. Sci.* 5 (2012) 7936–7942. <https://doi.org/10.1039/C2EE21802J>.
7 4 [98] I. Matanovic, K. Artyushkova, P. Atanassov, Understanding PGM-free catalysts by linking density
8 5 functional theory calculations and structural analysis: Perspectives and challenges, *Current Opinion*
9 6 *in Electrochemistry.* 9 (2018) 137–144. <https://doi.org/10.1016/j.coelec.2018.03.009>.
10 7 [99] S. Rojas-Carbonell, K. Artyushkova, A. Serov, C. Santoro, I. Matanovic, P. Atanassov, Effect of pH
11 8 on the Activity of Platinum Group Metal-Free Catalysts in Oxygen Reduction Reaction, *ACS Catal.*
12 9 8 (2018) 3041–3053. <https://doi.org/10.1021/acscatal.7b03991>.
13 10 [100] A. Serov, K. Artyushkova, P. Atanassov, Fe-N-C Oxygen Reduction Fuel Cell Catalyst Derived
14 11 from Carbendazim: Synthesis, Structure, and Reactivity, *Advanced Energy Materials.* 4 (2014)
15 12 1301735. <https://doi.org/10.1002/aenm.201301735>.
16 13 [101] R. Sgarbi, K. Kumar, F. Jaouen, A. Zitolo, E.A. Ticianelli, F. Maillard, Oxygen reduction reaction
17 14 mechanism and kinetics on M-N_xCy and M@N-C active sites present in model M-N-C catalysts
18 15 under alkaline and acidic conditions, *J Solid State Electrochem.* 25 (2021) 45–56.
19 16 <https://doi.org/10.1007/s10008-019-04436-w>.
20 17 [102] W. Zhong, Z. Wang, S. Han, L. Deng, J. Yu, Y. Lin, X. Long, M. Gu, S. Yang, Identifying the
21 18 Active Sites of a Single Atom Catalyst with pH-Universal Oxygen Reduction Reaction Activity,
22 19 *Cell Reports Physical Science.* 1 (2020) 100115. <https://doi.org/10.1016/j.xcrp.2020.100115>.
23 20 [103] S. Rojas-Carbonell, C. Santoro, A. Serov, P. Atanassov, Transition metal-nitrogen-carbon catalysts
24 21 for oxygen reduction reaction in neutral electrolyte, *Electrochemistry Communications.* 75 (2017)
25 22 38–42. <https://doi.org/10.1016/j.elecom.2016.12.011>.
26 23 [104] D. Singh, J. Tian, K. Mamtani, J. King, J.T. Miller, U.S. Ozkan, A comparison of N-containing
27 24 carbon nanostructures (CN_x) and N-coordinated iron-carbon catalysts (FeNC) for the oxygen
28 25 reduction reaction in acidic media, *Journal of Catalysis.* 317 (2014) 30–43.
29 26 <https://doi.org/10.1016/j.jcat.2014.05.025>.
30 27 [105] M. Muhyuddin, N. Zocche, R. Lorenzi, C. Ferrara, F. Poli, F. Soavi, C. Santoro, Valorization of the
31 28 inedible pistachio shells into nanoscale transition metal and nitrogen codoped carbon-based
32 29 electrocatalysts for hydrogen evolution reaction and oxygen reduction reaction, *Mater Renew*
33 30 *Sustain Energy.* 11 (2022) 131–141. <https://doi.org/10.1007/s40243-022-00212-5>.
34 31 [106] M. Muhyuddin, D. Testa, R. Lorenzi, G.M. Vanacore, F. Poli, F. Soavi, S. Specchia, W. Giurlani,
35 32 M. Innocenti, L. Rosi, C. Santoro, Iron-based electrocatalysts derived from scrap tires for oxygen
36 33 reduction reaction: Evolution of synthesis-structure-performance relationship in acidic, neutral and
37 34 alkaline media, *Electrochimica Acta.* 433 (2022) 141254.
38 35 <https://doi.org/10.1016/j.electacta.2022.141254>.
39 36 [107] C.H. Choi, C. Baldizzone, J.-P. Grote, A.K. Schuppert, F. Jaouen, K.J.J. Mayrhofer, Stability of Fe-
40 37 N-C Catalysts in Acidic Medium Studied by Operando Spectroscopy, *Angew Chem Int Ed Engl.* 54
41 38 (2015) 12753–12757. <https://doi.org/10.1002/anie.201504903>.
42 39 [108] Q. Ma, H. Jin, J. Zhu, Z. Li, H. Xu, B. Liu, Z. Zhang, J. Ma, S. Mu, Stabilizing Fe-N-C Catalysts as
43 40 Model for Oxygen Reduction Reaction, *Advanced Science.* 8 (2021) 2102209.
44 41 <https://doi.org/10.1002/advs.202102209>.
45 42 [109] T.J. Omasta, L. Wang, X. Peng, C.A. Lewis, J.R. Varcoe, W.E. Mustain, Importance of balancing
46 43 membrane and electrode water in anion exchange membrane fuel cells, *Journal of Power Sources.*
47 44 375 (2018) 205–213. <https://doi.org/10.1016/j.jpowsour.2017.05.006>.
48 45 [110] W.E. Mustain, Understanding how high-performance anion exchange membrane fuel cells were
49 46 achieved: Component, interfacial, and cell-level factors, *Current Opinion in Electrochemistry.* 12
50 47 (2018) 233–239. <https://doi.org/10.1016/j.coelec.2018.11.010>.
51 48 [111] N. Ramaswamy, S. Mukerjee, Alkaline Anion-Exchange Membrane Fuel Cells: Challenges in
52 49 Electrocatalysis and Interfacial Charge Transfer, *Chem. Rev.* 119 (2019) 11945–11979.
53 50 <https://doi.org/10.1021/acs.chemrev.9b00157>.
54
55
56
57
58
59
60
61
62
63
64
65

- 1
2
3
4 1 [112] P. Teppor, R. Jäger, M. Paalo, A. Adamson, M. Härmas, O. Volobujeva, J. Aruväli, R. Palm, E.
5 2 Lust, Peat as a carbon source for non-platinum group metal oxygen electrocatalysts and AEMFC
6 3 cathodes, *International Journal of Hydrogen Energy*. 47 (2022) 16908–16920.
7 4 <https://doi.org/10.1016/j.ijhydene.2022.03.199>.
8 5
9 6 [113] J. Lilloja, M. Mooste, E. Kibena-Pöldsepp, A. Sarapuu, B. Zulevi, A. Kikas, H.-M. Piirsoo, A.
10 7 Tamm, V. Kisand, S. Holdcroft, A. Serov, K. Tammeveski, Mesoporous iron-nitrogen co-doped
11 8 carbon material as cathode catalyst for the anion exchange membrane fuel cell, *Journal of Power
12 9 Sources Advances*. 8 (2021) 100052. <https://doi.org/10.1016/j.powera.2021.100052>.
13 10
14 11 [114] M. Hao, R. Dun, Y. Su, L. He, F. Ning, X. Zhou, W. Li, In situ self-doped biomass-derived porous
15 12 carbon as an excellent oxygen reduction electrocatalyst for fuel cells and metal–air batteries, *J.
16 13 Mater. Chem. A*. 9 (2021) 14331–14343. <https://doi.org/10.1039/D1TA01417J>.
17 14
18 15 [115] L. Wang, M. Bellini, H.A. Miller, J.R. Varcoe, A high conductivity ultrathin anion-exchange
19 16 membrane with 500+ h alkali stability for use in alkaline membrane fuel cells that can achieve 2 W
20 17 cm⁻² at 80 °C, *J. Mater. Chem. A*. 6 (2018) 15404–15412. <https://doi.org/10.1039/C8TA04783A>.
21 18
22 19 [116] P.G. Santori, F.D. Speck, S. Cherevko, H.A. Firouzjaie, X. Peng, W.E. Mustain, F. Jaouen, High
23 20 Performance FeNC and Mn-oxide/FeNC Layers for AEMFC Cathodes, *J. Electrochem. Soc.* 167
24 21 (2020) 134505. <https://doi.org/10.1149/1945-7111/abb7e0>.
25 22
26 23 [117] H. Adabi, A. Shakouri, N. Ul Hassan, J.R. Varcoe, B. Zulevi, A. Serov, J.R. Regalbuto, W.E.
27 24 Mustain, High-performing commercial Fe–N–C cathode electrocatalyst for anion-exchange
28 25 membrane fuel cells, *Nat Energy*. 6 (2021) 834–843. <https://doi.org/10.1038/s41560-021-00878-7>.
29 26
30 27 [118] Md.M. Hossen, Md.S. Hasan, Md.R.I. Sardar, J. bin Haider, Mottakin, K. Tammeveski, P.
31 28 Atanassov, State-of-the-art and developmental trends in platinum group metal-free cathode catalyst
32 29 for anion exchange membrane fuel cell (AEMFC), *Applied Catalysis B: Environmental*. (2022)
33 30 121733. <https://doi.org/10.1016/j.apcatb.2022.121733>.
34 31
35 32 [119] X. Peng, V. Kashyap, B. Ng, S. Kurungot, L. Wang, J.R. Varcoe, W.E. Mustain, High-Performing
36 33 PGM-Free AEMFC Cathodes from Carbon-Supported Cobalt Ferrite Nanoparticles, *Catalysts*. 9
37 34 (2019) 264. <https://doi.org/10.3390/catal9030264>.
38 35
39 36 [120] H. Adabi, P.G. Santori, A. Shakouri, X. Peng, K. Yassin, I.G. Rasin, S. Brandon, D.R. Dekel, N.U.
40 37 Hassan, M.-T. Sougrati, A. Zitolo, J.R. Varcoe, J.R. Regalbuto, F. Jaouen, W.E. Mustain,
41 38 Understanding how single-atom site density drives the performance and durability of PGM-free Fe–
42 39 N–C cathodes in anion exchange membrane fuel cells, *Materials Today Advances*. 12 (2021)
43 40 100179. <https://doi.org/10.1016/j.mtadv.2021.100179>.
44 41
45 42 [121] J. Woo, S.Y. Yang, Y.J. Sa, W.-Y. Choi, M.-H. Lee, H.-W. Lee, T.J. Shin, T.-Y. Kim, S.H. Joo,
46 43 Promoting Oxygen Reduction Reaction Activity of Fe–N/C Electrocatalysts by Silica-Coating-
47 44 Mediated Synthesis for Anion-Exchange Membrane Fuel Cells, *Chem. Mater.* 30 (2018) 6684–
48 45 6701. <https://doi.org/10.1021/acs.chemmater.8b02117>.
49 46
50 47 [122] Y. Yang, X. Xu, P. Sun, H. Xu, L. Yang, X. Zeng, Y. Huang, S. Wang, D. Cao, AgNPs@Fe-N-C
51 48 oxygen reduction catalysts for anion exchange membrane fuel cells, *Nano Energy*. 100 (2022)
52 49 107466. <https://doi.org/10.1016/j.nanoen.2022.107466>.
53 50
54 51 [123] W. Xu, D. Yoon, Y. Yang, Y. Xiong, H. Li, R. Zeng, D.A. Muller, H.D. Abruña, MOF-Derived
55 52 Bimetallic Pd–Co Alkaline ORR Electrocatalysts, *ACS Appl. Mater. Interfaces*. 14 (2022) 44735–
56 53 44744. <https://doi.org/10.1021/acsami.2c10074>.
57 54
58 55 [124] S. Das, S. Ghosh, T. Kuila, N.C. Murmu, A. Kundu, Biomass-Derived Advanced Carbon-Based
59 56 Electrocatalysts for Oxygen Reduction Reaction, *Biomass*. 2 (2022) 155–177.
60 57 <https://doi.org/10.3390/biomass2030010>.
61 58
62 59
63 60
64 61
65 62